

Air Force Institute of Technology

**AFIT Scholar**

---

Theses and Dissertations

Student Graduate Works

---

3-2021

## Static Fatigue of Hi-Nicalon™ S Ceramic Fiber Tows at 600°C in Air and Silicic Acid-Saturated Steam

Caleigh M. Nelson

Follow this and additional works at: <https://scholar.afit.edu/etd>



Part of the [Ceramic Materials Commons](#), and the [Structures and Materials Commons](#)

---

### Recommended Citation

Nelson, Caleigh M., "Static Fatigue of Hi-Nicalon™ S Ceramic Fiber Tows at 600°C in Air and Silicic Acid-Saturated Steam" (2021). *Theses and Dissertations*. 5069.

<https://scholar.afit.edu/etd/5069>

This Thesis is brought to you for free and open access by the Student Graduate Works at AFIT Scholar. It has been accepted for inclusion in Theses and Dissertations by an authorized administrator of AFIT Scholar. For more information, please contact [AFIT.ENWL.Repository@us.af.mil](mailto:AFIT.ENWL.Repository@us.af.mil).



**STATIC FATIGUE OF HI-NICALON™ S CERAMIC FIBER TOWS AT 600°C IN  
AIR AND SILICIC ACID-SATURATED STEAM**

THESIS

Caleigh M. Nelson, Second Lieutenant, USAF

AFIT-ENY-MS-21-M-309

**DEPARTMENT OF THE AIR FORCE  
AIR UNIVERSITY**

**AIR FORCE INSTITUTE OF TECHNOLOGY**

**Wright-Patterson Air Force Base, Ohio**

**DISTRIBUTION STATEMENT A.  
APPROVED FOR PUBLIC RELEASE; DISTRIBUTION UNLIMITED.**

The views expressed in this thesis are those of the author and do not reflect the official policy or position of the United States Air Force, Department of Defense, or the United States Government. This material is declared a work of the U.S. Government and is not subject to copyright protection in the United States.

AFIT-ENY-MS-21-M-309

STATIC FATIGUE OF HI-NICALON™ S CERAMIC FIBER TOWS AT 600°C IN  
AIR AND SILICIC ACID-SATURATED STEAM

THESIS

Presented to the Faculty

Department of Aeronautics and Astronautics

Graduate School of Engineering and Management

Air Force Institute of Technology

Air University

Air Education and Training Command

In Partial Fulfillment of the Requirements for the  
Degree of Master of Science in Aeronautical Engineering

Caleigh M. Nelson, BS

Second Lieutenant, USAF

March 2021

**DISTRIBUTION STATEMENT A.**  
APPROVED FOR PUBLIC RELEASE; DISTRIBUTION UNLIMITED.

AFIT-ENY-MS-21-M-309

STATIC FATIGUE OF HI-NICALON™ S CERAMIC FIBER TOWS AT 600°C IN  
AIR AND SILICIC ACID-SATURATED STEAM

Caleigh M. Nelson, BS

Second Lieutenant, USAF

Committee Membership:

Dr. Marina B. Ruggles-Wrenn  
Chair

Dr. Randall S. Hay  
Member

Dr. Eric Jones  
Member

### **Abstract**

Ceramic matrix composites (CMCs) have the potential to be utilized in applications such as hypersonic vehicles, aircraft leading edges, hot sections of engines, and rocket nozzles. Of particular interest are advanced SiC/SiC composites that can withstand the elevated temperatures and harsh oxidizing environments while maintaining their properties and structural integrity under an applied load. Steam, a major component of combustion environment, is one such aggressive oxidizing environment. As steam passes through the SiC/SiC composite, entering the composite interior through the cracks in the SiC matrix, it becomes saturated with silicic acid,  $\text{Si}(\text{OH})_4$ . Before incorporating SiC/SiC composites in the next generation aerospace engines, the long-term impacts of exposure to the aggressive saturated steam environment on the composite durability must be thoroughly examined and understood. An in-depth understanding of the composite performance demands an in-depth study and understanding of the performance of the reinforcing SiC fibers. This study investigates the static fatigue of Hi-Nicalon<sup>TM</sup> S SiC fiber tows at an intermediate temperature of 600°C in laboratory air and in silicic acid-saturated steam. The fiber tow consists of 500 fiber filaments with an average diameter of 13  $\mu\text{m}$ . Static fatigue tests were performed at applied stresses ranging from 2.96 MPa to 1300 MPa. Run-out was defined as survival of 100 h at applied stress. The presence of saturated steam significantly degraded the static fatigue performance of the fiber tows at 600°C. The static fatigue lifetimes of the Hi-Nicalon<sup>TM</sup> S SiC fiber tows were decreased by one order of magnitude due to silicic acid-saturated steam.

## **Acknowledgments**

I would like to express my sincere appreciation to my faculty advisor, Dr. Marina Ruggles-Wrenn, for her guidance and support throughout the course of this thesis effort. Her insight and experience were certainly appreciated. I would, also, like to thank the lab technicians, M.R. and J.S., for their expertise, continual support, and guidance over the course of the year. Without their knowledge, problem solving abilities, and endless encouragement, this thesis would not have been possible.

Finally, I would like to thank my husband for his patience, love, and unending support. I am blessed to have you in my life and am excited for this to be the start of our adventure together. OL.

Caleigh M. Nelson

## Table of Contents

|  | Page |
|--|------|
| Abstract.....  | iv   |
| Table of Contents.....   | vi   |
| List of Figures.....   | viii |
| List of Tables.....  | xi   |
| I. Introduction.....   | 1    |
| II. Background.....  | 4    |
| Chapter Overview.....  | 4    |
| 2.1 Ceramic Matrix Composites (CMCs).....                                  | 4    |
| 2.2 Silicon Carbide-Based Fibers.....                                      | 9    |
| 2.3 Weaknesses of CMCs and SiC-based fibers.....                           | 14   |
| 2.4 Past Work.....   | 20   |
| 2.5 Research Objectives.....   | 22   |
| III. Methodology.....  | 23   |
| Chapter Overview.....  | 23   |
| 3.1 Material and Equipment.....  | 23   |
| 3.2 Specimen Preparation Procedure.....                                    | 27   |
| 3.3 Experimental Facility Operations.....                                  | 30   |
| IV. Analysis and Results.....  | 34   |
| 4.1 Temperature Profiles.....  | 34   |
| 4.2 Engineering Strain Measurement.....                                    | 36   |
| 4.3 Static Fatigue of Hi-Nicalon <sup>TM</sup> S Fiber Tows at 600°C.....  | 40   |
| 4.4 Microstructural Analysis of Hi-Nicalon <sup>TM</sup> S Fiber Tows..... | 53   |
| V. Conclusions and Recommendations.....                                    | 53   |

|  |    |
|--|----|
| 5.1 Conclusions .....                        | 53 |
| 5.2 Recommendations for Future Research..... | 54 |
| Bibliography .....                           | 56 |

## List of Figures

|   | Page |
|---|------|
| Figure 1 : Strength to weight ratio for select materials versus temperature. Reproduced from [3] with kind permission from Elsevier.....  | 3    |
| Figure 2 : Representative Stress-Strain Curves: Monolithic Ceramic vs. CMC, reproduced from [4] .....   | 6    |
| Figure 3 : Current Design Philosophies for Damage Tolerant CMCs: a) damage tolerant design concept showing uncorrelated fiber failure, debonding, and pullout b) fiber coating with weak fiber/matrix interface, c) porous matrix, and d) fugitive coating [8], reproduced with permission from Wiley ..... | 7    |
| Figure 4 : Composites reinforced by (a) particles, (b) whiskers, and (c) continuous fibers  | 8    |
| Figure 5 : Oxide scale formation of Hi-Nicalon <sup>TM</sup> S fiber exposed to silicic acid-saturated steam, reproduced from [12] .....  | 11   |
| Figure 6 : Production process for Hi-Nicalon <sup>TM</sup> S SiC fibers by electron irradiation curing and pyrolysis. Reproduced with kind permission from Springer Science & Business Media B.V. pg. 117, Figure 8. Copyright c 2005 by Springer-Verlag Berlin Heidelberg. [13] .....                      | 12   |
| Figure 7: Microstructures of three generations of Nicalon <sup>TM</sup> fibers. Reproduced with kind permission from Springer Science & Business Media B.V. pg. 118, Figure 9. Copyright c 2005 by Springer-Verlag Berlin Heidelberg. [13] .....  | 13   |
| Figure 8 : Oxidation-induced subcritical crack growth in SiC-based fibers reproduced from [14] with kind permission from Wiley .....  | 16   |
| Figure 9 : Creep regimes, reproduced from [17] .....  | 17   |

Figure 10 : A spool of Hi-Nicalon™ S fiber tow, manufactured by Nippon Carbon Co., Ltd. [26]..... 24

Figure 11 : MHI HGA-S-CX1300 heater (a) and controller (b). Reproduced from [24]. 26

Figure 12 : Three tab method layout, reproduced from [24] ..... 28

Figure 13 : Fiber specimen preparation steps. Reproduced from [12] ..... 30

Figure 14 : Test specimen mounted in creep testing apparatus. Reproduced from [23] .. 31

Figure 15 : Alumina susceptor and steam feed tube assembled in one half of the furnace. Reproduced from [4] ..... 32

Figure 16 : Bleed-off assembly located just prior to the feeding tube of the test chamber. Reproduced from [29] ..... 33

Figure 17 : Silica wool within alumina tube acting as saturation chamber for silicic acid-saturated steam. Reproduced from [29] ..... 34

Figure 18 : Assembled saturated steam test configuration. Reproduced from [29]..... 34

Figure 19 : Temperature Profile at 600° C in air ..... 35

Figure 20 : Temperature Profile at 600° C in saturated steam..... 36

Figure 21 : Representative strain vs. time curves for Hi-Nicalon™ S fiber tows at 600°C at 1023 MPa in (a) air and (b) saturated steam ..... 43

Figure 22 : Representative strain vs. time curves for Hi-Nicalon™ S fiber tows at 600°C at 1157 MPa in (a) air and (b) saturated steam ..... 45

Figure 23 : Representative strain vs. time curves for Hi-Nicalon™ S fiber tows at 600°C at 1257 MPa in (a) air and (b) saturated steam ..... 45

Figure 24 : Representative strain vs. time curves for Hi-Nicalon™ S fiber tows at 600°C at 1300 MPa in (a) air and (b) saturated steam ..... 46

Figure 25 : Representative strain vs. time curves for Hi-Nicalon™ S fiber tows at 600°C  
in air ..... 46

Figure 26 : Representative strain vs. time curves for Hi-Nicalon™ S fiber tows at 600°C  
in air. Time scale is truncated to highlight strain vs. time behavior during early  
portion of each test ..... 47

Figure 27 : Representative strain vs. time curves for Hi-Nicalon™ S fiber tows at 600°C  
in saturated steam ..... 47

Figure 28 : Representative strain vs. time curves for Hi-Nicalon™ S fiber tows at 600°C  
in air. Time scale is truncated to highlight strain vs. time behavior during early  
portion of each test ..... 48

Figure 29 : Strain rates vs. applied stress for Hi-Nicalon™ S fiber tows at 600°C in both  
air and saturated steam ..... 49

Figure 30 : Applied stress vs. time to rupture obtained for Hi-Nicalon™ S at 600°C in air  
and saturated steam. Arrow indicates that specimen failure did not occur when the  
test was terminated. .... 52

## List of Tables

|  | Page |
|--|------|
| Table 1 : Military and Commercial applications for CMCs, reproduced from [1].....  | 5    |
| Table 2 : Advantages of various reinforced CMCs, reproduced from [1].....  | 8    |
| Table 3 : Properties of Silicon Carbide-Based Fibers reproduced from [14] with kind<br>permission from Wiley.....  | 14   |
| Table 4 : Creep mechanisms in fine-grained polycrystalline ceramics. Adapted from [4]<br>.....   | 19   |
| Table 5 : Typical properties of Hi-Nicalon <sup>TM</sup> S fiber. Data reproduced from NGS<br>Advanced Fibers Co., Ltd. [28][12].....  | 25   |
| Table 6 : Effective lengths calculated in air and saturated steam at 600°C.....  | 39   |
| Table 7 : Summary of tensile static fatigue test results obtained for Hi-Nicalon <sup>TM</sup> S fiber<br>tows at 600°C in laboratory air and in silicic acid-saturated steam..... | 42   |
| Table 8 : Comparison of stress exponents obtained for the Hi-Nicalon <sup>TM</sup> S fiber tows at<br>intermediate temperatures in air and saturated steam.....                    | 51   |

# STATIC FATIGUE OF HI-NICALON™ S CERAMIC FIBER TOWS AT 600°C IN AIR AND SILICIC ACID-SATURATED STEAM

## I. Introduction

In the material industry, there is a push to utilize composite materials in lieu of traditional metal alloys due to their superior material properties and customizable qualities. A composite material is defined as a material composed of two or more distinct phases [1]. As composite material research continues to advance today with space-age materials, processes, and challenges, the field can take pride in tracing its roots of experimentation and development back to early civilizations. For example, the houses and buildings constructed in the Ancient Egyptian and Mesopotamian era were built with bricks composed of a mixture of mud, clay, and straw [2]. Additionally, in 1200 AD Mongols, under command of Genghis Khan, created composite bows using wood, bone, and “animal glue” [2]. Continual developments in the material field have led to advancements in technology and improved performance of material-based applications. Such advancements in materials have influenced the evolution from historical Ages of Stone, Bronze, and Iron, to the modern-day Age of Composites.

Significant innovations in composite materials can be traced back to the 20<sup>th</sup> century when a transition from natural composites to synthetic or man-made composites occurred. The development of polymer resins and the improvements made to specialized molding processes helped to shape the current composite industry. By 1935, Owens Corning manufactured fiberglass—an extremely strong and lightweight material—eventually utilized for aircraft skin panels and shields for electronic radar equipment during WWII [2]. This plastic polymer and glass fiber mixture laid the foundation for the

fiber reinforced polymer (FRP) industry. Carbon fibers were developed in the 1960s. Silicon Carbide (SiC) fibers, which are widely considered for present-day application with ceramic matrix composites, were developed in the 1980s.

Ceramic matrix composites (CMCs) are appropriate in several areas, especially in the aerospace field where environments with high operating temperatures and exposure to moisture are experienced. Such environments are found in turbine engines; thus, CMC utilization has become an attractive option for the industry. Operating at higher temperatures is beneficial to turbine engines as it allows for an increase in engine efficiency, a decrease in fuel consumption, and fewer emissions released as a by-product. Because of their superior ability to withstand extreme temperatures, operate in moisture rich environments with minimal corrosion, low specific weight, and the reduced need for cooling air [3], CMCs are a prime candidate for replacing metal alloys in turbine engine combustion chambers. Figure 1 illustrates the temperature limits of CMCs, as well as the strength to weight ratios of various metal alloys and CMCs.

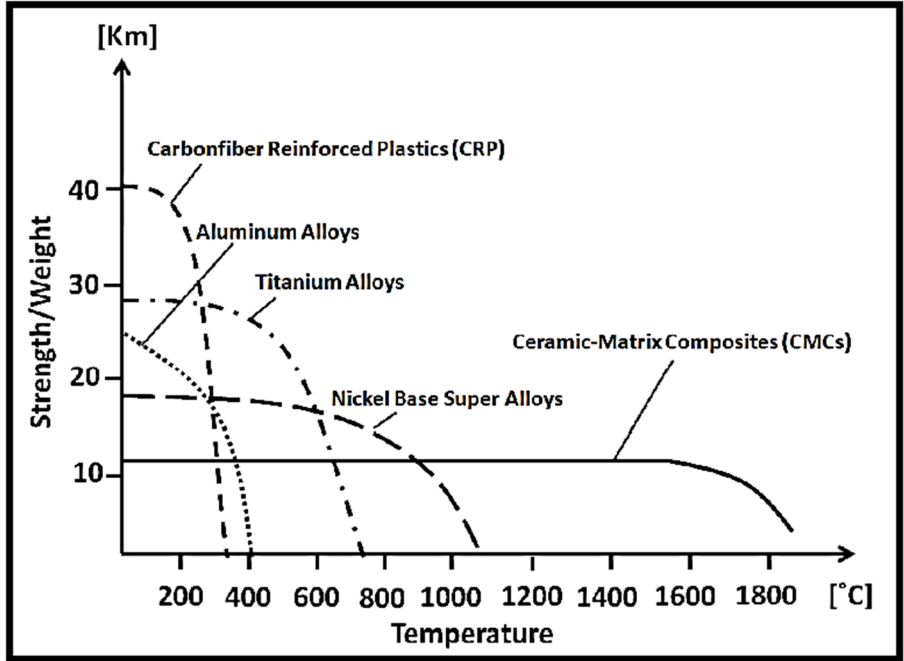


Figure 1 : Strength to weight ratio for select materials versus temperature. Reproduced from [3] with kind permission from Elsevier

## **II. Background**

### **Chapter Overview**

The purpose of this chapter is to go into further detail of the development, applications, benefits, and drawbacks of CMCs and Silicon Carbide-based fibers. Section 2.1 explains the development and current applications of Ceramic Matrix Composites (CMCs). Section 2.2 provides an overview of Silicon Carbide (SiC) based fibers with a focus on the fabrication processes of the near stoichiometric Hi-Nicalon™ S fibers and their resulting material properties and behaviors. In Section 2.3, the weaknesses of CMCs and SiC based fibers will be discussed. These weaknesses include degradation by oxidation and creep effects. Observations and past work on this topic will be discussed in Section 2.4, specifically highlighting the efforts from AFIT Alumni. Finally, Section 2.5 details the research objectives and motivation for this research and its significance for today's material and aerospace industries.

### **2.1 Ceramic Matrix Composites (CMCs)**

Ceramic matrix composites (CMCs) have been an area of research interest for several decades. Beginning in the mid-20<sup>th</sup> century, developments in CMCs have driven technological advancements. The transition from metal alloys to CMCs is due to the attractive material properties and behaviors recorded for composite materials such as high strength, low density, resistance to oxidation, and the capability to withstand extreme temperatures and environments [3]. Because of these superior properties, CMCs are commonly used in aerospace applications such as hypersonic vehicles, rocket nozzles,

combustion chambers, and leading edges of aircraft [1], [3]. Table 1 outlines additional applications of CMCs in both the military and commercial sectors.

**Table 1 : Military and Commercial applications for CMCs, reproduced from [1]**

| Applications/<br>Sectors   | Continuous Fiber CMCs   |   |  |
|----------------------------|---|---|--|
| <b>Military</b>            | <ul style="list-style-type: none"> <li>• F414 and F110 Nozzle Flaps and Seals</li> <li>• F117 Aft Deck Heat Shields</li> <li>• Engine Vanes</li> <li>• Flame Holders</li> </ul> | <ul style="list-style-type: none"> <li>• Orbital Transfer Engine Thrusters</li> <li>• Low Cost Large Rocket Thruster (Million Pound) Heavy Lift Launch</li> <li>• Tactical Missile Combustors, Rotors</li> <li>• Divert Attitude and Control Thrusters</li> </ul> | <ul style="list-style-type: none"> <li>• Turboramjet Variable Area Nozzles</li> <li>• Surveillance OTV Thrusters</li> <li>• Hypersonic Leading Edges, Inlet Cowlings and Nozzles</li> <li>• Linear Aerospike, Engine, Thrust Cells and Ramp</li> </ul> |
| <b>Commercial/Dual Use</b> | <ul style="list-style-type: none"> <li>• Heat Exchangers</li> <li>• Radiant Burner Tubes</li> <li>• Land-Based Gas Turbines</li> <li>• Candle Filters</li> </ul>                | <ul style="list-style-type: none"> <li>• MDH Air Preheater Tubes</li> <li>• Immersion Heaters</li> <li>• Seal-less Magnetic Pumps</li> <li>• Motorcycle Brakes</li> </ul>   | <ul style="list-style-type: none"> <li>• Diesel Components</li> <li>• Valve Guides</li> <li>• Pistons</li> <li>• Turbochargers Rotors</li> </ul>   |

Although CMCs are prime candidates for applications shown in Table 1, ceramics are known for their brittle nature and catastrophic failure mode. A tangible example of a monolithic ceramic is a piece of pottery. As one may imagine, when exposed to an applied stress or aggressive environment, these ceramic materials are deemed unserviceable due to shattering, or catastrophic failure. Due to the significance of each component within an engine, it would be hazardous to incorporate ceramic material in these specific applications. Figure 2 is a schematic of general stress-strain curves for both a monolithic ceramic and a CMC. This schematic illustrates the catastrophic or immediate failure seen by ceramic materials.

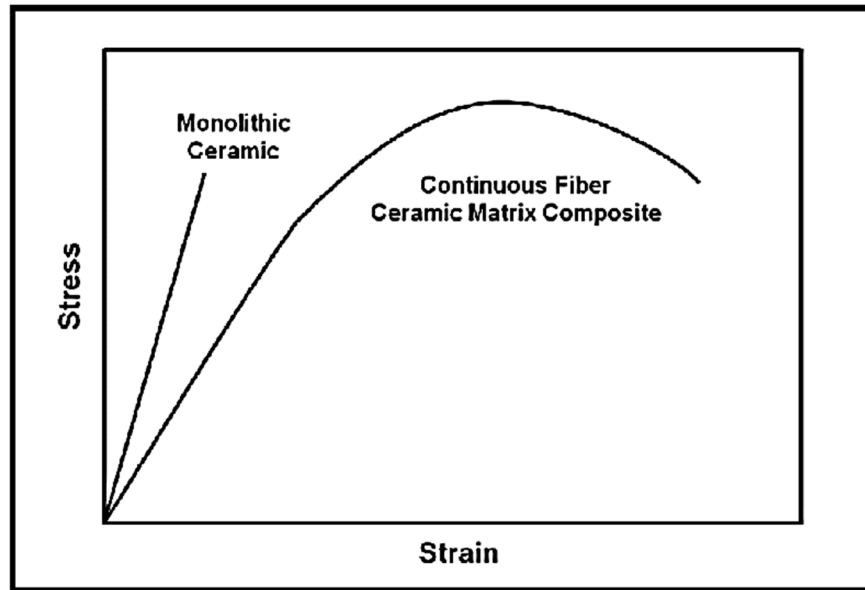
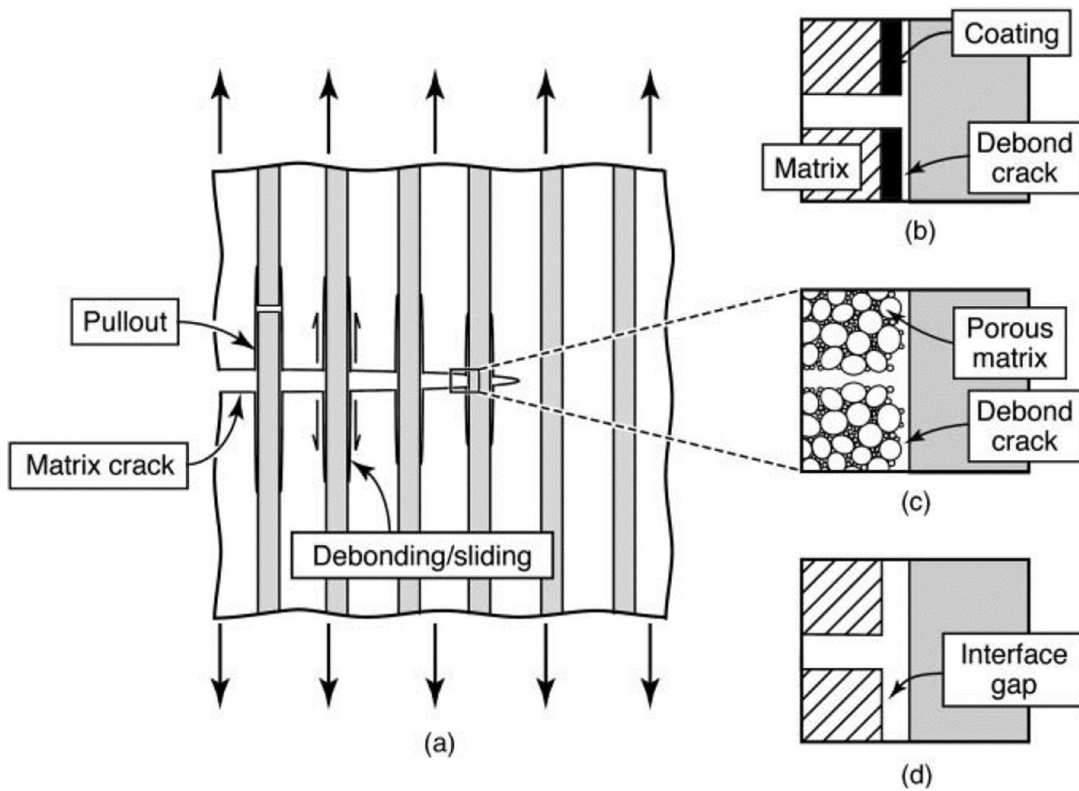


Figure 2 : Representative Stress-Strain Curves: Monolithic Ceramic vs. CMC, reproduced from [4]

On the other hand, CMCs are more damage tolerant than monolithic ceramics, as seen by the continued deformation and eventual failure on the stress-strain diagram (Figure 2). This damage tolerance is due to the reinforcing fibers within the matrix of the composite material. Reinforcing fibers, depending on their orientation, withstand and transfer a large portion of the applied load, which results in a “graceful”, delayed failure by promoting crack deflection. The matrix portion of the composite, however, serves to hold the fibers in place while simultaneously acting as the primary medium that contains cracks deflected away from the load bearing fibers. For instance, in the case of porous-matrix oxide-oxide composites, the porosity of a matrix helps to absorb the energy of the crack which promotes the failure of the matrix, not the fibers [5]. In the case of dense-matrix CMCs, if a crack encounters a weak interface between the matrix and the fibers, such as a fiber coating, the crack is deflected and the fibers remain intact [5], [6]. Figure

3 depicts the phenomena of fiber pull-out and the crack deflection caused by fiber coating, porous matrix, and weak interphase.

Additionally, CMCs exhibit improved fracture toughness—a material’s ability to resist a crack without brittle failure occurring—compared to monolithic ceramics, again contributing to graceful failure [7].



**Figure 3 : Current Design Philosophies for Damage Tolerant CMCs: a) damage tolerant design concept showing uncorrelated fiber failure, debonding, and pullout b) fiber coating with weak fiber/matrix interface, c) porous matrix, and d) fugitive coating [8], reproduced with permission from Wiley**

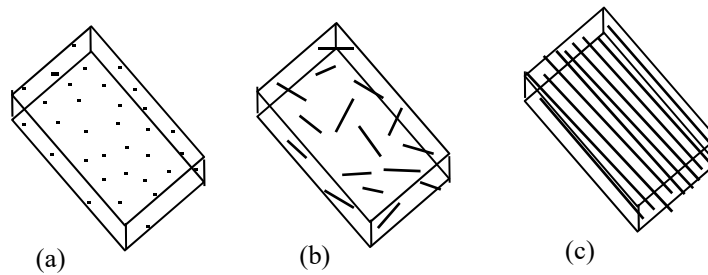


**Figure 4 : Composites reinforced by (a) particles, (b) whiskers, and (c) continuous fibers**

There are two major categories of composite reinforcements: continuous and discontinuous. Figure 4 (a, b) displays discontinuous reinforcements. Figure 4 (c) shows continuous fibers. Continuous reinforcements use long, continuous fibers like yarn or woven fabric, while discontinuous reinforcements consist of particles or short, whisker-like fibers [1], [6], [7]. Advantages of CMCs with continuous and discontinuous reinforcements are summarized in Table 2.

**Table 2 : Advantages of various reinforced CMCs, reproduced from [1]**

| <b>Continuous CMCs</b>  | <b>Discontinuous CMCs</b>   |
|---|---|
| Excellent High Temp Mech. Properties  | Excellent High Temp Mech. Properties                              |
| High Specific Strength and Stiffness<br>High Fracture Toughness                               | High Specific Strength and Stiffness<br>Higher Useful Strengths   |
| Dimensional Stability<br>Low Thermal Expansion  | Fracture Toughness Good but Inferior to Continuous CMCs           |
| Good Thermal Shock Resistance<br>Graceful Failure Mode  | Thermal Shock Resistance<br>Inferior to Continuous CMCs           |
| Oxidation Resistance<br>Machining More Difficult<br>Processing More Complicated and Expensive | Amenable to Cheaper Conventional Processes<br>Machining Expensive |

## **2.2 Silicon Carbide-Based Fibers**

The performance of a CMC strongly depends on the selected fiber reinforcement. Understanding the mechanical behavior and the failure mechanisms of fibers is critical to the design of CMCs [9]. As discussed in Section 2.1, fibers are essential to the strength of a CMC, as they are responsible for carrying a large percentage of the load experienced by the composite. As a result, it is imperative to understand the effects that severe environments have on the fibers, their material properties, and mechanical response. This point is further emphasized by Lamon et al., “The sensitivity of fibers toward temperature and environmental effects is a factor of primary importance for the development of composites with durable load carrying capacity.” [10]. To fully understand mechanical properties, behaviors, and failure mechanisms of Silicon Carbide (SiC)-based fibers, it is important to note the generational advancements seen in the processing of SiC fibers.

### **2.2.1 History of SiC-Based Fibers**

Silicon Carbide (SiC) fibers—researched extensively within the academic community—stand out as the fiber of the future in high temperature applications due to their high crystalline structure and near-stoichiometric composition [9]. Produced in Japan by Nippon Carbon Co, the first generation of SiC fibers—denoted as Nicalon™ fibers—were developed in 1980. The fibers were fabricated by the melting and spinning of polycarbosilane precursor into ceramic fibers [11]. This fabrication method proved to be faulty for producing fibers with a uniform diameter. The Nicalon™ fibers experienced creep effects at elevated temperatures due to interactions between grain boundaries, as well as degradation from oxidation [11]. To reduce oxidation, the carbon content of the

fibers needed to be reduced to achieve a more stoichiometric composition. Thus, a new fabrication process was needed, and the second-generation fiber was born.

The second-generation fiber, known as Hi-Nicalon<sup>TM</sup>, was indeed more stoichiometric than the previous generation. The reduction in oxygen and carbon content was accomplished by radiation cross-linking. As a result, the Hi-Nicalon<sup>TM</sup> fibers were 35% stiffer and the strength retention at elevated temperatures improved [11]. Silica growth was present on the surfaces of the fibers; this was observed in the earlier generation because of carbon oxidation after exposure to an oxidizing environment. The silica scale was determined to slow the internal degradation of the fiber, which in turn, prolonged the fiber's lifetime. A micrograph of a SiC-based fiber shows the silica scale growth in Figure 5. This image was taken using Scanning Electron Microscopy (SEM) technology. In addition to the added stiffness and strength, the Hi-Nicalon<sup>TM</sup> fibers demonstrated lower creep rates and an increased Young's modulus [11].

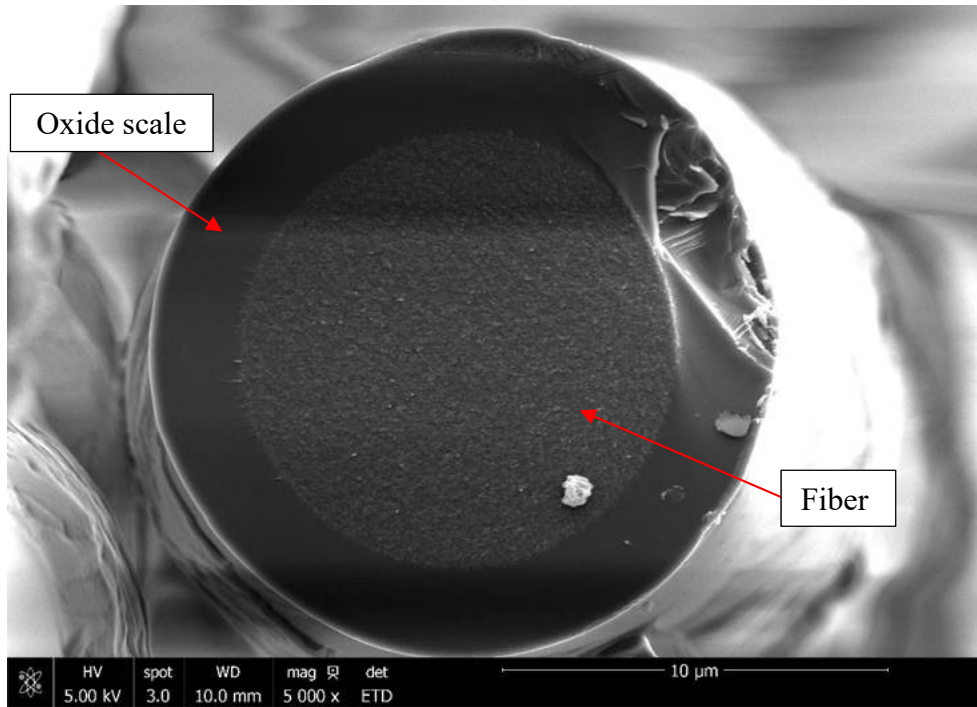


**Figure 5 : Oxide scale formation of Hi-Nicalon™ S fiber exposed to silicic acid-saturated steam, reproduced from [12]**

With oxidation still being a primary inhibitor to the fibers' strength, a third-generation fiber was created. This fiber is known as Hi-Nicalon™ S. The S denotes the near stoichiometric carbon composition of 1.05, limiting the number of free carbons in the material. The stoichiometry was achieved by heat treating the fiber up to 1500°C. The fabrication process of Hi-Nicalon™ S fibers is shown in Figure 6.

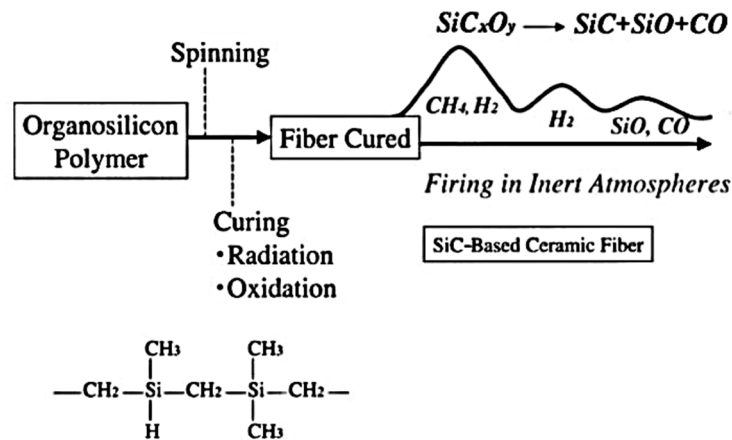
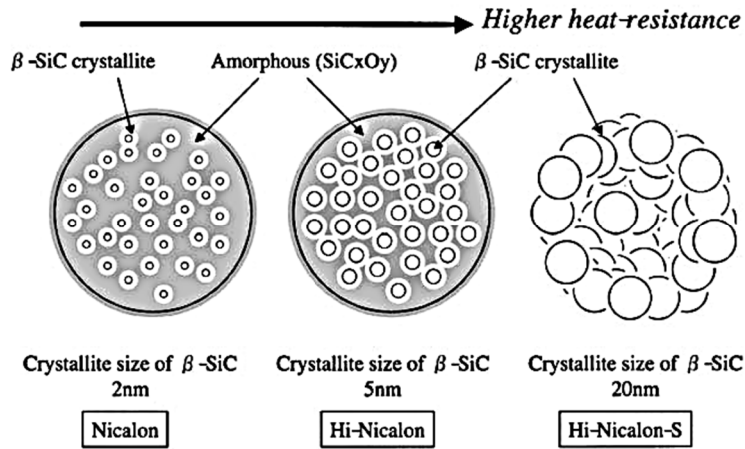


Figure 6 : Production process for Hi-Nicalon™ S SiC fibers by electron irradiation curing and pyrolysis. Reproduced with kind permission from Springer Science & Business Media B.V. pg. 117, Figure 8. Copyright c 2005 by Springer-Verlag Berlin Heidelberg. [13]

Following the trend of improved material properties and mechanical behaviors, the third-generation fiber's performance superseded that of the other generations. Hi-Nicalon™ S fibers had a higher creep resistance due to the heat treatment and were more resistant to slow crack growth due to their lack of free carbon [10]. As the fabrication processes of the Nicalon™ fibers evolved, the microstructure of the fibers followed suit. The fiber diameter became smaller as time went on, after experimentation concluded that the larger the diameter, the weaker the fiber [9]. The larger the diameter, the more likely the fiber will have surface or internal defect that would result in premature fracture. Additionally, the grain sizes of the fibers enlarged which contributed to the creep resistance mentioned earlier. The change in grain size and fiber diameter are depicted in Figure 7 for each of the three fiber types.



**Figure 7: Microstructures of three generations of Nicalon™ fibers. Reproduced with kind permission from Springer Science & Business Media B.V. pg. 118, Figure 9. Copyright c 2005 by Springer-Verlag Berlin Heidelberg. [13]**

From Table 3 one may observe the improvement of material properties between the three generations of Nicalon™ fibers. For example, the Young's modulus of Nicalon™ fibers compared to Hi-Nicalon™ S fibers increased from 200 GPa to 420 GPa, respectively. Because of the improved properties listed below and their potential for survival in both elevated temperatures and oxidizing environments, Hi-Nicalon™ S fibers and other near stoichiometric SiC-based fibers are prime candidates for selection of CMC components in aerospace applications. Hi-Nicalon™ S fibers will be the focus of this research.

**Table 3 : Properties of Silicon Carbide-Based Fibers reproduced from [14] with kind permission from Wiley**

| Fiber                            | NLM202         | Hi-Nicalon       | Hi-Nicalon S   | Tyranno SA3     |
|----------------------------------|----------------|------------------|----------------|-----------------|
| Diameter ( $\mu\text{m}$ )       | 15             | 14               | 12             | 7.5             |
| at.% Si                          | 39.5           | 41.6             | 48.7           | 46–49           |
| at.% C                           | 48.5           | 57.8             | 51             | 53–51           |
| at.% O                           | 12             | 0.6              | 0.2            | <0.4            |
| at.% Al                          | 0              | 0                | 0              | <0.2            |
| at.% C/ at.% Si                  | 1.32           | 1.41             | 1.05           | 1.15–1.04       |
| CTE ( $10^{-6} \text{ K}^{-1}$ ) | 3.1 (RT–500°C) | 4.6 (200°–800°C) | 5.1 (RT–500°C) | 4.5 (RT–1000°C) |
| Density ( $\text{kg/m}^3$ )      | 2550           | 2740             | 3100           | 3100            |
| Young's modulus (GPa)            | 200            | 270              | 420            | 380             |
| Tensile strength (MPa)           | 3000           | 2800             | 2600           | 2840            |
| Average grain size of SiC (nm)   | 5              | 10               | 20             | 50–100          |
| Free C                           |                |                  |                |                 |
| $L_a$ (nm)                       | <2             | 2–3              | 1–30           | Not available   |
| $N$                              | 2              | 5–8              |                |                 |

CTE, Coefficient of Thermal Expansion.

### 2.3 Weaknesses of CMCs and SiC-based fibers

Two of the primary weaknesses experienced by CMCs and SiC fibers are creep effects and degradation by oxidation. Both phenomena decrease the material's properties and contribute to premature fracture. Creep is defined as the deformation of a material when subjected to a constant load over time. Oxidation occurs as atomic elements in the material react with oxygen in the air, to produce oxides. These oxides break down the material which decreases the material's strength due to loss of physical matter, and endangers the overall performance of CMC [15]. Degradation by oxidation and observed creep behavior have been noticed in several research efforts and will be a primary focus in this work and will be further discussed in Section 2.3.1 and Section 2.3.2.

#### 2.3.1 Oxidation

The fibers and matrix of a CMC are both susceptible to oxidation. According to Halbig and Eckel, "A fiber's susceptibility to oxidation is influenced by the activation

energy of the carbon-oxygen reaction, impurities, pressure, temperature, carbon surface, and crystal structure.” Additionally, microcracks in the matrix contribute to oxidation of the fibers by allowing a path for the oxygen to travel to the fibers. Experimental observations led to the discovery of the relationship between applied stress and oxidation rates. It was noted that the greater the applied load, the greater the oxidation rate, resulting in a decrease in the material’s lifetime [14]–[16]. Also contributing to oxidation is the concentration of carbon and the grain size of the fibers. The increased percentage of free carbons increases the likelihood of oxidation as well as the smaller grain size of the fibers. Both of these factors decrease the lifetime of the material, as seen below [14]:

|             |              |   |               |   |             |   |          |
|-------------|--------------|---|---------------|---|-------------|---|----------|
| Lifetime:   | Tyranno SA3  | > | Hi-Nicalon™ S | > | Hi-Nicalon™ | > | Nicalon™ |
| Free carbon | (~2%)        |   | (~3%)         |   | (~17%)      |   | (~15 %)  |
| Grain size: | (~50—100 nm) |   | (~20 nm)      |   | (~10 nm)    |   | (~5 nm)  |

The presence and oxidation of free carbons within a fiber also allow for further crack growth. Cracks generate an internal stress that contributes to the fiber’s fracture under an increased load. See Figure 8 for a visual representation of oxidation-induced subcritical crack growth.

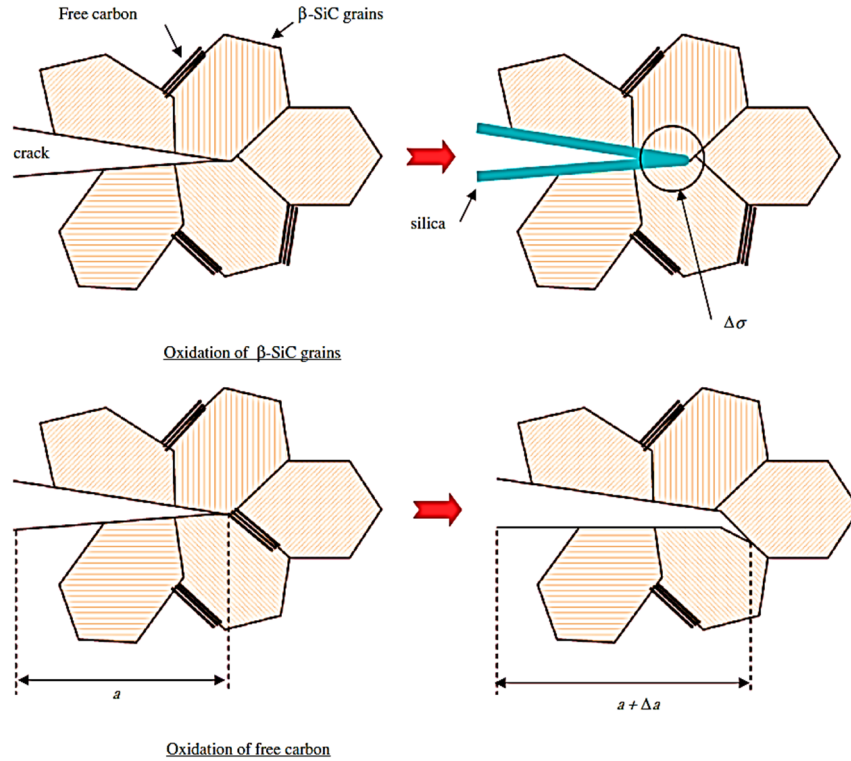


**Figure 8 : Oxidation-induced subcritical crack growth in SiC-based fibers reproduced from [14] with kind permission from Wiley**

There are two types of oxidation: passive and active. Active oxidation, dependent on steam flow rate, forms a volatile oxide which attacks the SiC. On the contrary, passive oxidation, independent of steam flow rate, forms an oxide layer that protects the fiber from environmental attack [16]. Generally, the occurrence of passive oxidation is preferred due to the generated layer of protection for the fiber.

### 2.3.2 Creep

The understanding of creep behavior of a material is foundational when the material is expected to undergo a constant stress over a long period of time. Without this knowledge, it is difficult to predict the general behavior and lifetime of the component.

This information is especially important for components utilized in engines or applications where the failure of a component would be deemed catastrophic to the performance of the system.

There are three creep regimes a material may experience when subjected to a constant load over time: primary, secondary, and tertiary.

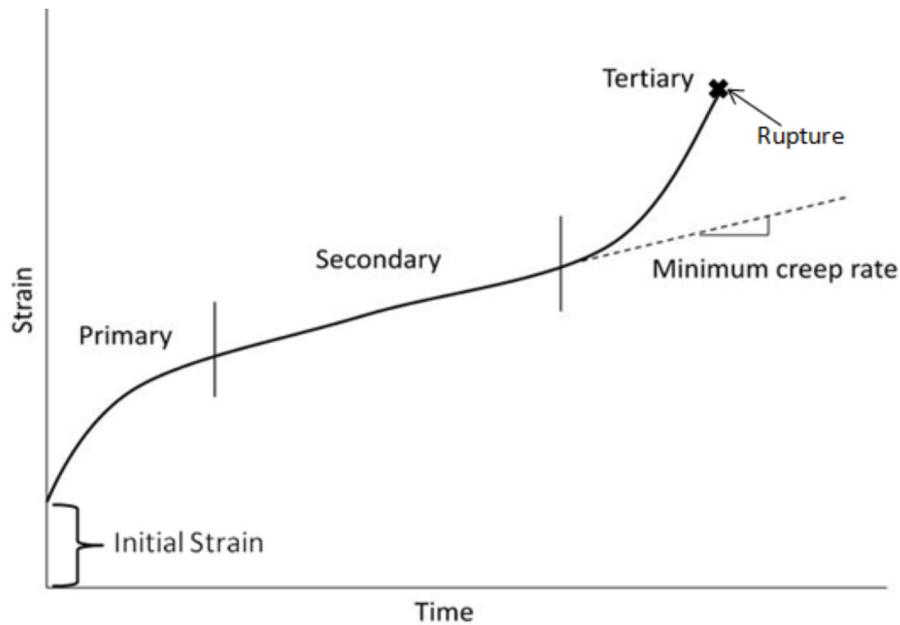


**Figure 9 : Creep regimes, reproduced from [17]**

The first regime, noted in Figure 9 as the primary or transient stage, is where the strain rate continually decreases over either a short or long period of time. This can be due to stress redistribution or changes in the microstructure, such as the grain size. The secondary stage represents a constant strain rate due to deformation of the microstructure of the material, in the case of this research, the fiber's microstructure. The final stage is known as the tertiary or rupture stage. During this stage, the strain rate increases

exponentially, resulting in voids, cracks, and eventually failure itself [6], [7], [17]. The secondary or steady-state region is of most importance for CMCs and can result from a variety of creep mechanisms at elevated temperatures. These various creep mechanisms can be seen in Table 4. The commonly known creep rate equation is derived from the Arrhenius rate equation [18]:

$$\dot{\varepsilon} = B \frac{D\mu b}{kT} \left(\frac{b}{d}\right)^p \left(\frac{\sigma}{\mu}\right)^n \quad (1)$$

where  $\dot{\varepsilon}$  is the strain rate,  $B$  is a constant,  $\mu$  is the shear modulus,  $b$  is the Burgers vector,  $k$  is the Boltzmann's constant,  $T$  is the absolute temperature,  $d$  is the grain size diameter,  $p$  is the grain size power law exponent,  $\sigma$  is the applied stress, and  $n$  is the stress power law exponent.  $D$  is the diffusion coefficient which is defined as:

$$D = D_o \exp\left(\frac{-Q}{RT}\right) \quad (2)$$

where  $D_o$  is a frequency factor,  $R$  is the universal gas constant,  $Q$  is the creep activation energy, and  $T$  is the absolute temperature.

From Equation (1), the variables  $n$  and  $p$  can be determined from experimental creep data, thus identifying the creep mechanism present in the test specimen. Values of  $n$  and  $p$  are present in Table 4. Diffusional creep and grain boundary sliding are the two mechanisms that dominate creep behavior of ceramics at elevated temperatures.

**Table 4 : Creep mechanisms in fine-grained polycrystalline ceramics. Adapted from [4]**

| $N$<br>stress exponent | $p$<br>grain size exponent | Mechanism  |
|------------------------|----------------------------|--|
| 1                      | 2                          | Diffusional creep through lattice (Nabarro-Herring creep)      |
| 1                      | 3                          | Diffusional creep along grain boundaries (Coble creep)         |
| 2                      | 1                          | Grain boundary sliding and interface-reaction controlled creep |
| 4                      | 3                          | GBS and cavity growth  |
| 3-5                    | 0                          | Dislocation creep: 3 –glide controlled, 5 – climb controlled   |
| >5                     | -                          | Cavity growth-controlled creep                                 |

Diffusional creep—creep due to mass transport—can be broken down into two subsets: Nabarro-Herring creep and Cobble creep. Nabarro-Herring creep is the diffusion that takes place through the grains, while Cobble creep occurs along the grain boundaries [18]. In both cases, grains elongate in the direction of the applied stress. Grain boundary sliding, as the name suggests, occurs as whole grains move with respect to one another to avoid or relieve local stresses. The result of this movement is elongation. Materials with smaller grain sizes tend to creep due to grain boundary sliding because the grains can more easily slide past each other. Typically, the lesser of the two mechanisms will control the creep strain rate [19].

It was found experimentally that creep resistance improved with the heat treatment of ceramic fibers such as Hi-Nicalon™ S. If the material was treated at a temperature higher than that of the operating temperature, it resulted in a greater

resistance to creep. Also, the grain size and the composition at or near the grain boundaries influence the increase in creep resistance. The experimental results referenced in this section can be further examined in the work of Sha et. al.

## **2.4 Past Work**

Numerous efforts have been made by researchers to contribute to the understanding of the mechanical behavior of SiC fibers in extreme environments. Lamon et al., Hay et al., and dozens of other researchers, including those from the Air Force Institute of Technology (AFIT), have dedicated their time and resources to better understand the creep behavior and degradation by oxidation of Hi-Nicalon<sup>TM</sup> S fibers over a range of temperatures. The observations recorded from past work at AFIT will be discussed in this section.

Armani [4] analyzed the creep of oxide fibers in air and steam environments at elevated temperatures. Through his work, a test facility was created to observe such behavior and effects on the fibers. Armani concluded that the presence of steam decreased the creep lifetimes and the steady-state creep rates of the Nextel<sup>TM</sup> fibers examined at temperatures ranging from 1100°C to 1300°C.

Steffens [20] later modified the specimen preparation procedure and the test facility for an experimental study concerning Hi-Nicalon<sup>TM</sup> S fiber tows at 800° C and 1100°C in both air and steam environments. The results at 800° C showed that the presence of steam degraded the creep lifetimes and creep strain rates of the Hi-Nicalon<sup>TM</sup> S fiber tows; however, at 1100° C the creep lifetimes and creep strain rates of the fiber tow increased by a magnitude of one. The improvement in creep performance seen at

1100° C was predicted to be from a protective silicon oxide scale that had formed on the outer edges of the fibers. The silicon scale delayed the growth of surface defects on the fiber specimen which ultimately delayed the fiber's fracture.

The investigative research of Hi-Nicalon™ S fibers at elevated temperatures in air and steam environments continued as Shillig tested specimens in both conditions at temperatures ranging from 800° C to 1100° C [21]. Shillig recorded the same trend in creep performance of the fiber tows. The fiber tow's creep lifetimes and creep strain rates were degraded in the steam condition, but this phenomenon was less prevalent as the temperature increased. Shillig also noticed that the fiber specimens were failing below the gauge section near the steam inlet. There were two mechanisms of oxidation—active and passive—occurring on the specimens. The passive oxidation formed a silicon oxide layer on the top portion of the fiber tow specimen, while the bottom portion of the fiber tow specimen was subjected to active oxidation. Shillig observed that when the steam entered the test chamber through the steam inlet tube located at the bottom of the susceptor, the steam was gradually leaching silica from the SiC fibers which saturated the steam with silicic acid. This chemical change of the steam contributed to the two oxidation mechanisms observed from the fibers.

The presence of chemically altered steam within the furnace sparked a modification of future testing conditions for Hi-Nicalon™ S fiber tows. Instead of testing in unsaturated steam, Robertson [17] and Sprinkle [22] developed a method to preheat the steam to the desired test temperature and saturate the steam with silicic acid prior to its deliverance into the test chamber. Robertson and Sprinkle's method of pre-saturating the steam included loading the alumina tube that runs along the length of the two heater units

with silica wool, allowing the generated steam the opportunity to become completely saturated with silicic acid before reaching the SiC fibers. This process eliminated the active oxidation problem and created a testing condition that better represented what the fibers would experience in a typical combustion environment.

The research efforts that followed Robertson's contribution adopted the steam saturation process and continued to test in this environment. Hi-Nicalon™ S fiber tows have been tested in air and in silicic acid-saturated steam at temperatures ranging from 700° C to 1100° C. Such experiments were conducted by Piper [23], Mitchell [24], Kroeger [25], and Gumucio [12]. It was found that the silicic acid-saturated steam had a detrimental impact on the fiber tow's creep performance, however not as severely as previous work tested at similar temperatures in unsaturated steam. This is due to the enhanced growth of the protective silica oxide layer resulting from the interaction between the silicic acid-saturated steam and the SiC fiber tow. The contributions and experimental results outlined in this section have laid the foundation for the specimen preparation procedures, testing methods, and facility operations utilized in this research effort.

## **2.5 Research Objectives**

This experimental study aims to further advance the documented research of Silicon Carbide fibers. A fiber tow of roughly 500 Hi-Nicalon™ S fibers with an average diameter of 13 μm will be used for experimentation during this research effort. The cross-sectional area was calculated to be  $6.63 \times 10^{-8} \text{ m}^2$  and this value was used in all engineering stress calculations. The overall objective is to document the mechanical

behavior and performance—specifically the static fatigue behavior and oxidation—of Hi-Nicalon™ S fibers in air and silicic acid-saturated steam environments at 600°C.

Previously, this fiber tow has been tested in the steam conditions mentioned above, across a temperature range between 700° C to 1100° C. The data and results gathered at the 600°C testing temperature will aid in the construction of the operating regime for this specific fiber type and provide more information about phenomena that occur at intermediate temperatures. Moreover, it will contribute to an understanding of the interaction between static fatigue and oxidation processes.

### **III. Methodology**

#### **Chapter Overview**

The purpose of this chapter is to discuss the material used in this effort, the equipment available for testing, and the operating procedures. The fiber specimen preparation process is outlined in Section 3.2. The Experimental Facility Operating procedures are covered in Section 3.3.

#### **3.1 Material and Equipment**

This research studied the static fatigue of Hi-Nicalon™ Type-S fiber tows at 600°C in laboratory air and silicic acid-saturated steam. The Hi-Nicalon™ S fiber, pictured in Figure 10, is the third-generation of SiC-based fiber manufactured by Nippon Carbon Co. in Tokyo, Japan [26]. The third-generation fiber proved to have superior material properties compared to its predecessors. These improvements in material properties are a result of the evolution of the fiber fabrication process. Hi-Nicalon™ S

fibers are fabricated by utilizing de-carbonization pyrolysis and electron-beam curing [27]. This process produces a near-stoichiometric fiber that has a greater resistance to oxidation, improved creep resistance, and yields a higher modulus while exposed to elevated temperatures, unlike the first and second generation Nicalon™ fibers [9].



**Figure 10 : A spool of Hi-Nicalon™ S fiber tow, manufactured by Nippon Carbon Co., Ltd. [26]**

The fiber tow utilized in this research consisted of approximately 500 filaments with an average diameter of 13  $\mu\text{m}$  [34]. Based on this data, a cross sectional area of  $6.63 \times 10^{-8} \text{ m}^2$  was used for all engineering stress calculations. The typical properties of Hi-Nicalon™ S fibers can be found in Table 5.

**Table 5 : Typical properties of Hi-Nicalon™ S fiber. Data reproduced from NGS Advanced Fibers Co., Ltd. [28][12]**

|                             |     |
|-----------------------------|-----|
| Number of filaments         | 500 |
| Filament diameter (μm)      | 13  |
| Product Form                | Tow |
| Sizing Agent                | PVA |
| Linear density, tex (g/km)  | 195 |
| Oxygen content (wt%)        | 0.8 |
| Modulus of Elasticity (GPA) | 380 |

The Hi-Nicalon™ S fiber test specimens were tested in the Mechanics of Advanced Aerospace Materials Laboratory of the Department of Aeronautics and Astronautics at AFIT. The fiber tow testing facility was originally created by Armani [4] but was later modified by Steffens [20], Shillig [21], Robertson [17], and Sprinkle [22]. The modified facility can observe the creep behavior of fiber specimens in air and in steam (saturated and unsaturated) conditions at various temperatures. The test facility is composed of several components that aid in achieving the desired testing environments and allows for accurate observation of the fiber specimen's creep behavior. Testing in a silicic acid-saturated steam environment replicates what the SiC fibers would experience in a SiC/SiC composite exposed to a combustion environment. When steam enters cracks found in the matrix of the SiC/SiC composite, silica is leached from the matrix which then saturates the steam with silicic acid before it reaches the reinforcing SiC fibers of the composite [24], [29].

For testing in steam environments, a Cole Parmer ® model 7518-10 peristaltic pump connects a 50-gallon reservoir of deionized water to a steam generator (Model HGA-S-01, MHI, Cincinnati, OH). The deionized water is the primary source for steam

generation, with the flow rate set according to the operating temperature of the test. Two CX1300 heating units (see Figure 11(a)) are connected in series, both powered by an IBPAN controller (see Figure 11(b)). These heating units ensure the steam is at the appropriate testing temperature before it enters the test chamber. The heating units and their connection points are covered with insulation (KVS 174/400, RATH, Newark, DE) to minimize the amount of heat lost to the ambient air. An alumina tube runs through the heating chamber and acts as a reducing nozzle. The diameter of the tube reduces from 50 mm to 6 mm. The 6 mm diameter end of the alumina tube connects to an alumina supply tube which delivers the steam to the test chamber. A R-type thermocouple, sheathed in alumina, is inserted into a fitted-hole on the side of the supply tube to monitor the steam's temperature just before it enters the test chamber. To saturate the steam, silica wool (Hereaus Quartz, LLC USA, Austin TX) is packed into the 50 mm diameter portion of the alumina tube in a manner that enables the steam to permeate the wool, producing steam now saturated with silicic acid.

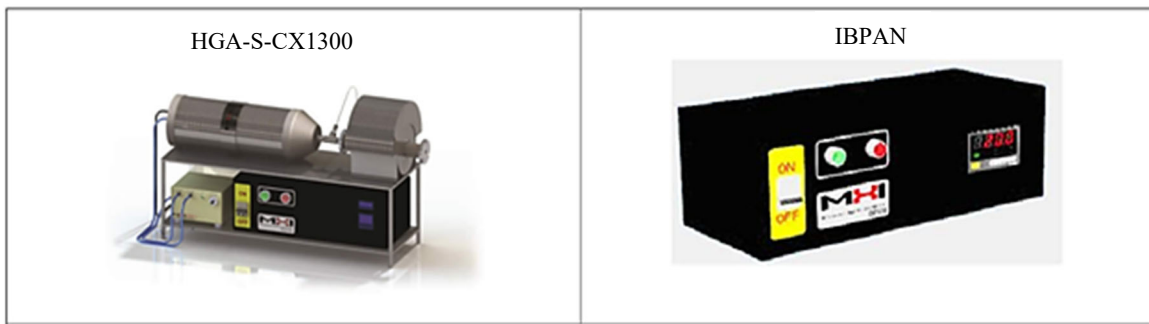


**Figure 11 : MHI HGA-S-CX1300 heater (a) and controller (b). Reproduced from [24]**

A compact two-zone resistance-heated furnace (Model 653.03A, MTS Systems Corporation, Eden Prairie, MN) with two temperature controllers (MTS 409.83) provides the elevated temperature environment for the fiber tow specimen. A K-type thermocouple gathers temperature data over the length of the furnace and generates a temperature profile for air and steam conditions. A ceramic susceptor fitted within the furnace allows for a more repeatable and distributed temperature along the test specimen. The ceramic susceptor is an alumina tube with two end caps and a hole along the side that the steam supply tube slides into, if desired. The fiber tow's gauge section is located inside the susceptor with the ends of the specimen exiting through the top and bottom slots of the susceptor's end caps.

In order to avoid high-temperature exposure to the fiber or other material, potentially resulting in a thermo-chemical reaction, a cold gripping method is used in all tests. Therefore, a LVDT (Schaevitz M12-30), attached to the bottom tab of the fiber tow, measures the specimen's elongation outside the furnace. A dead weight suspension system is utilized to apply a load to the fiber specimen for the creep test. The rod that supports the dead weight extends from the bottom of the LVDT. Displacement data from the LVDT is collected and recorded by an MTS FlexTest 40 digital controller.

### **3.2 Specimen Preparation Procedure**

The specimen preparation procedure has been modified over the years. Armani designed the first iteration of fiberglass tabs [4]. The method of affixing the fiber tow to the original two fiberglass tabs was modified after the phenomenon of fiber pull-out was observed. As a result, a third tab was introduced by Steffens to properly secure the fibers

within the fiberglass tabs [20]. Figure 12 depicts the three-tab method layout used in this study.

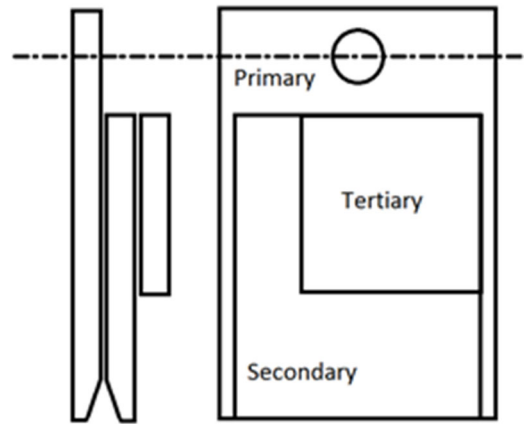


**Figure 12 : Three tab method layout, reproduced from [24]**

The dimensions of the primary, secondary, and tertiary tabs are 1.0 in x 1.5 in (0.0254 m x 0.0381 m), 1.0 in x 1.0 in (0.0254 m x 0.0254 m), and 0.75 in x 0.75 in (0.0191 m x 0.0191 m), respectively. Each tab is cut to the dimensions stated above and any sharp edges are sanded down to eliminate possible damage to the fibers during specimen preparation. The hole punched along the centerline of the primary tab is used to suspend the test specimen from the hook fixtures in the testing facility.

To begin the fiber specimen preparation process, the grid workstation, seen in Figure 13, was thoroughly wiped down using isopropanol. In step one, the primary tabs were secured to the grid surface 7 in apart using a piece of tape for each. Another piece of tape was placed on the workstation under the leading edge of the primary tabs to catch any spillage from the epoxy. After cutting a roughly 16 in section of fiber tow from the spool, the fibers are centered on the primary tab's punched hole and the workstation's

grid line (see step two). Following the alignment of the fibers, the fiber tow is adhered to the primary tab using a two-part epoxy (Hardman Double Bubble Epoxy, 04001) and the secondary tab (see step three). When placing the secondary tab onto the epoxy-covered fiber, avoid applying an excessive amount of force to the tab during the adherence process. Applying an excessive force to the tabs during fabrication introduces the risk of generating microcracks within the fibers, which will result in fiber pull-out from the tabs during the tensile creep test. Once the secondary tab has properly adhered, the fibers are gently folded over onto the secondary tab, ensuring there is a “dog ear” shape bend in the fibers. Allowing for this bend in the fibers ensures they are not tightly pressed against the potentially jagged edge of the tab, which could cause breakage. The final step, step 5 in Figure 13, is to bond the fibers between the secondary and tertiary tabs, and to cut the excess fiber from the ends of the test specimen using a single blade razor. Allow an hour for the epoxy to properly cure before removing and clearly labeling each specimen. Always handle the test specimens with care and ensure gloves are worn during and after the preparation process. A more in depth explanation of the specimen preparation procedure can be found in Appendix A1 of Steffens’ work [20].

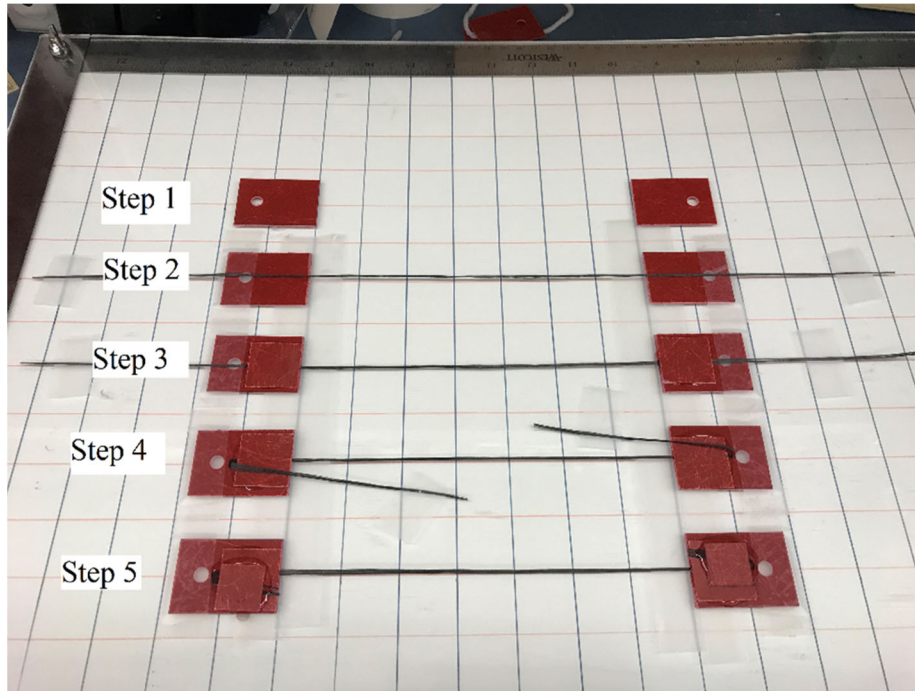


**Figure 13 : Fiber specimen preparation steps. Reproduced from [12]**

### **3.3 Experimental Facility Operations**

To conduct a tensile creep test in either air or steam environments, it is first required that the test specimen be properly loaded into the test chamber of the susceptor and furnace. To do so, attach one end of the test specimen to the upper hook fixture and feed the fibers through the susceptor via the slots of the susceptor's end caps, hooking the specimen's end tab to the lower hook on the testing facility. Once the fiber tow is in place within the susceptor, close the clam shells of the furnace, ensure the steam inlet tube is inserted into the susceptor and that there is sufficient insulation around the furnace and the supply tube insertion area. Set the furnace to the desired temperature and allow ample time for the test rig to achieve a uniform temperature within the susceptor. If testing in saturated or unsaturated steam, allow the generated steam to reach the test temperature before inserting the steam inlet tube into the bottom of the susceptor. As the furnace is

heating up, activate the fan which is attached to the testing rig. The fan helps to cool the top tab of the fiber tow specimen, preventing the yielding and failure of the fiber glass material due to the heat rising from the furnace. Once the test rig is operating at the appropriate temperature, carefully load a specified amount of weight onto the dead weight suspension rod using the load support. Begin collecting elongation measurements from the LVDT sensor and record the data using an MTS program. Figure 14 provides a visual representation of the test specimen properly mounted in the creep testing apparatus.

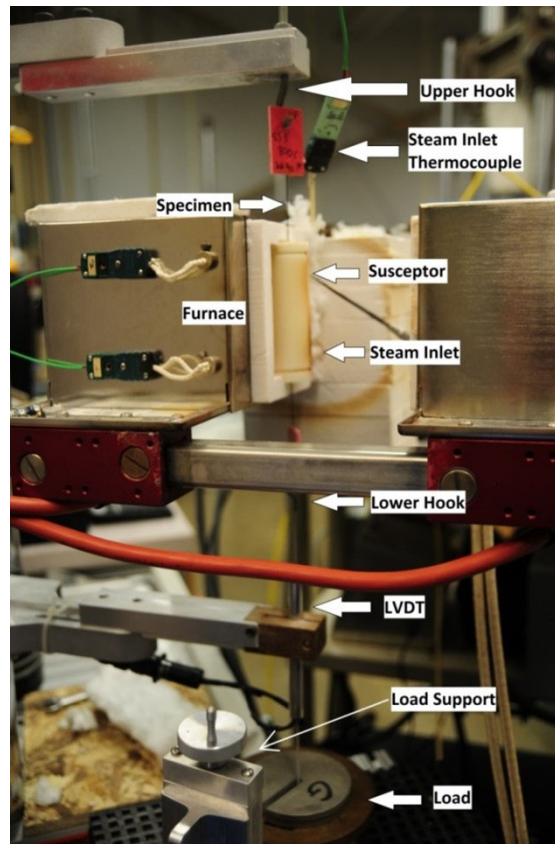


Figure 14 : Test specimen mounted in creep testing apparatus. Reproduced from [23]

If a steam environment is desired, the pump, steam generator, and the two CX1300 heaters must be turned on. The pump's flow rate of deionized water was set at 6.5 ml/min for the purposes of this study. The generated steam travels through the alumina tube located within the two heaters, where it is heated to the desired testing temperature before it is delivered to the test chamber. The continuously generated steam has a slightly positive pressure, expelling the dry air to create a uniform steam environment inside the susceptor via the steam supply tube. The steam supply tube is inserted into the bottom portion of the susceptor which allows the entire test chamber exposure to the steam environment (Figure 15). The bleed-off assembly located just before the steam supply tube, allows for the steam's flow rate to be controlled prior to its deliverance into the susceptor. The steam's flow rate is controlled by rotating the bleed-off tube. The bleed-off assembly is depicted in Figure 16.



**Figure 15 : Alumina susceptor and steam feed tube assembled in one half of the furnace.**

Reproduced from [4]

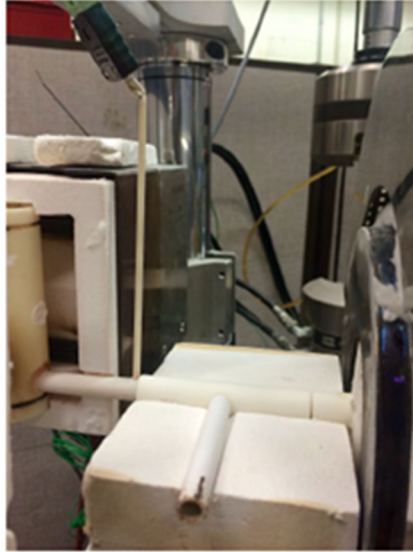


**Figure 16 : Bleed-off assembly located just prior to the feeding tube of the test chamber. Reproduced from [29]**

To saturate the steam, silica wool must be loaded into the alumina tube that runs along the two CX1300 heaters. The steam that is generated by the steam generator flows along the silica wool inside the alumina tube, also known as the saturation chamber, and becomes saturated with silicic acid. Figure 17 shows the silica wool packed into the alumina tube. The overall configuration of the test facility is shown in Figure 18.



Figure 17 : Silica wool within alumina tube acting as saturation chamber for silicic acid-saturated steam. Reproduced from [29]

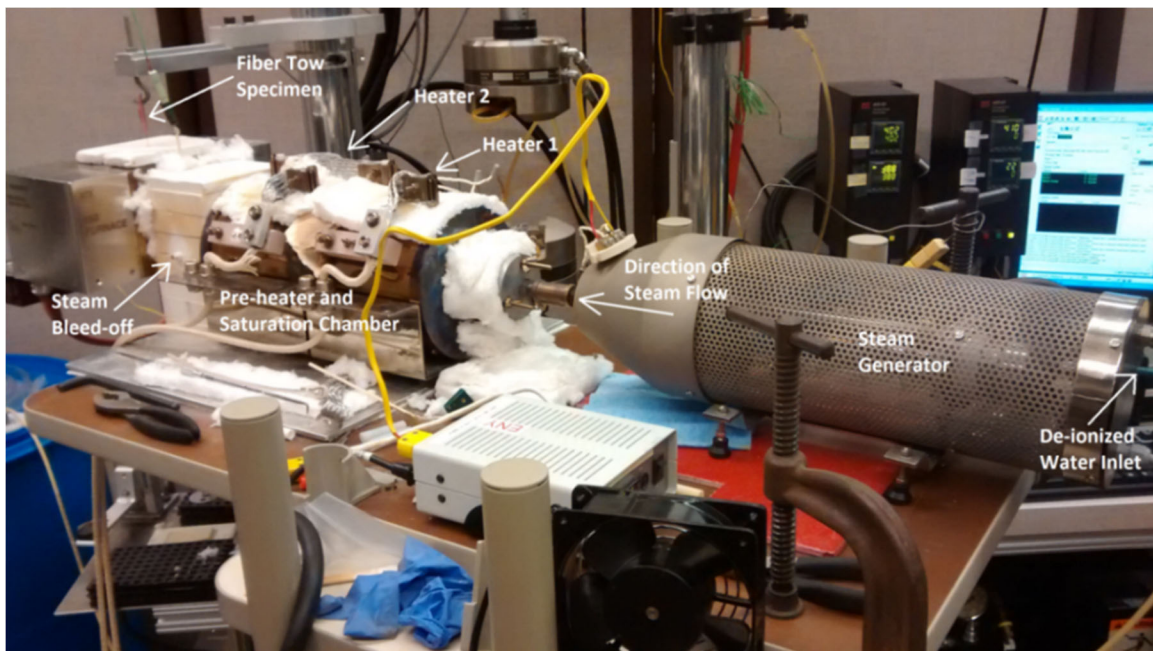


Figure 18 : Assembled saturated steam test configuration. Reproduced from [29]

## IV. Analysis and Results

### 4.1 Temperature Profiles

Before conducting a tensile creep test of the fiber specimens in air and in silicic acid-saturated steam, a temperature profile must be generated for both testing configurations to confirm the test chamber is experiencing a uniform testing temperature.

Additionally, the temperature profile data gathered in each air and steam condition helps to determine the effective gauge lengths, which are later used to calculate the accumulated strain and strain rate from the displacement values obtained by the LVDT for each test. The following section, Section 4.2, discusses the methods used to determine the effective gauge length and calculate the engineering strain.

To record the temperature data, a K-type thermocouple with accuracy of  $\pm 3^\circ\text{C}$  was attached to a hydraulic ram actuator of an MTS machine, which vertically displaced the thermocouple along the centerline of the susceptor within the furnace. The thermocouple recorded temperature readings with the MTS software. The temperature profiles for  $600^\circ\text{C}$  in air and in saturated steam are shown in Figure 19 and Figure 20, respectively.

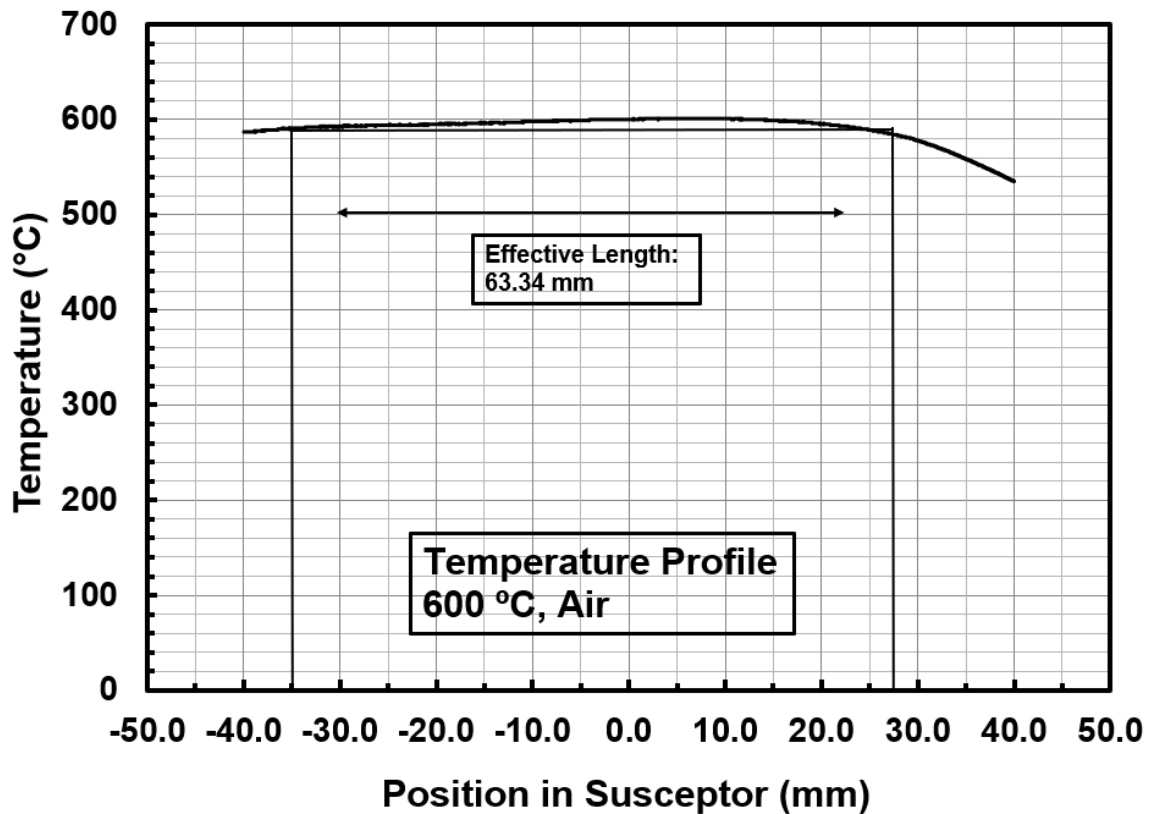


Figure 19 : Temperature Profile at  $600^\circ\text{C}$  in air

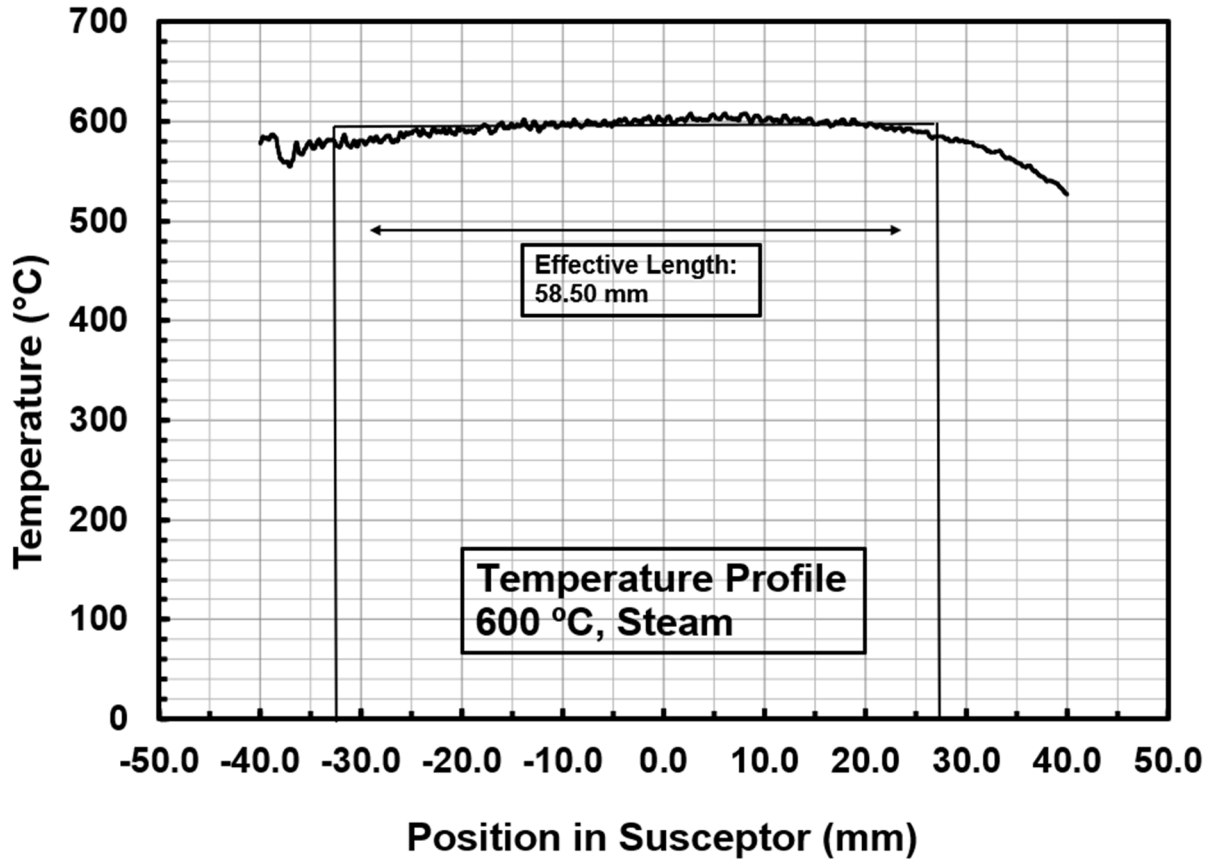


Figure 20 : Temperature Profile at 600° C in saturated steam

Note that in Figure 19 and Figure 20, the middle portion of the susceptor is positioned at 0 mm while the bottom and top ends of the susceptor correspond to a position of -40 mm and +40 mm, respectively.

#### 4.2 Engineering Strain Measurement

Numerous methods can be employed to measure strain. One method is to attach an extensometer to a specimen and directly measure its elongation, which can be used to calculate strain. Because an extensometer cannot be mounted onto the fiber tow an alternate method of obtaining a strain measurement was required.

As described in Section 3.3, a rod with a hook on the top end and a weight suspension system on the bottom end, runs through a linear variable displacement transducer (LVDT). The bottom tab of the fiber tow specimen gently hooks onto the rod, while an applied stress is placed on the weight suspension system. As the fibers deform, the LVDT externally records a summation of displacements experienced by the specimen throughout various temperature regions. There are three temperature regions that the fiber experiences: the cold zone, the temperature gradient, and the hot zone. The cold zone refers to the portions of the fiber tow that are outside of the furnace, exposed to ambient air. The temperature gradient region is located inside the furnace but outside of the hot zone. In this region, the fiber tow experiences a span of temperatures around that of the desired testing temperature. Lastly, the hot zone is denoted as the middle section of the furnace that is at the target temperature of 600°C. The total displacement data is then used to calculate the strain and strain rate of the specimen in a more indirect manner, as proposed by Armani [4]. However, before one can use the displacement data to calculate strain and strain rate, the effective gauge length of the specimen must be found. The effective gauge length of the specimen is the length in which the majority of the specimen's deformation will occur under a temperature profile, according to the temperature regions described above. The following equations represent the method proposed by Armani to calculate the effective gauge length value and were used to indirectly calculate the specimen's strain and strain rate for each case of applied stress.

Given a fiber tow specimen of length  $2L$  and denoting its center as the zero position, the creep experienced by the specimen occurs along its length from  $-L$  to  $L$ .

Outside of these bounds, the creep is considered negligible due to the lower temperature.

The creep strain and creep strain rate can be derived from the following:

$$\varepsilon_m = \frac{\Delta l}{2L} = \int_0^t \dot{\varepsilon}_m dt \quad (3)$$

$$\dot{\varepsilon}_m = \frac{\text{measured extension rate}}{2L} = \frac{1}{2L} \int_{-L}^L \dot{\varepsilon} dl \quad (4)$$

The total strain,  $\varepsilon_m$ , and total strain rate,  $\dot{\varepsilon}_m$ , calculated from Equation (3) and Equation (4), respectively, account for the variation of strain and its associated rate along the length of the fiber, due to variations in temperature. It is assumed that the fiber will deform the most in the hot zone, or center of the furnace, which is at the desired testing temperature. As a result of this assumption, the center section of the furnace will be denoted with the subscript  $0$  in the following equations. By integrating the strain rate at the center of the furnace with respect to time, the strain at the center of the furnace may be found. The strain at the center of the furnace may also be found by dividing the specimen's overall change in length,  $\Delta l$ , by the hypothetical length,  $(2L)_{eff}$ . The hypothetical length is also known as the effective gauge length. The strain at the target temperature can then be calculated:

$$\varepsilon_o = \int_0^t \dot{\varepsilon}_o dt = \frac{\Delta l}{(2L)_{eff}} \quad (5)$$

Similarly, the strain rate at the center of the furnace can be described in terms of effective gauge length as:

$$\dot{\varepsilon}_o = \frac{\text{measured extension rate}}{(2L)_{eff}} = \frac{1}{(2L)_{eff}} \int_{-L}^L \dot{\varepsilon} dl \quad (6)$$

Taking the ratio of Equation (4) and Equation (6) yields:

$$\frac{\dot{\varepsilon}_m}{\dot{\varepsilon}_o} = \frac{\Delta l}{(2L)_{eff}} \quad (7)$$

Because stress is constant along the length of the fiber tow and temperature varies along the length of the fiber tow, the general power-law creep equation can be applied:

$$\dot{\epsilon} = A\sigma^n \exp\left(\frac{-Q}{RT(l)}\right) \quad (8)$$

The ratio of measured strain rate to actual strain rate can be reduced to a function of temperature by combining Equation (4), Equation (7), and Equation (8):

$$\frac{\dot{\epsilon}_m}{\dot{\epsilon}_o} = \frac{1}{2L} \int_{-L}^L \exp\left\{\frac{-Q}{R}\left(\frac{1}{T(l)} - \frac{1}{T_o}\right)\right\} dl \quad (9)$$

Equation (9) can then be expressed as a summation of increments of length, h, where  $L=hk$ , and k is an integer:

$$\frac{\dot{\epsilon}_m}{\dot{\epsilon}_o} = \frac{1}{2k} \sum_{i=-k}^k \exp\left\{\frac{-Q}{R}\left(\frac{1}{T(l)} - \frac{1}{T_o}\right)\right\} \quad (10)$$

The effective gauge length can now be calculated from the numerical approach seen in Equation (10):

$$(2L)_{eff} = 2L \left(\frac{\dot{\epsilon}_m}{\dot{\epsilon}_o}\right) \quad (11)$$

Since the effective gauge length accounts for variations in temperature along the fiber tow, it can therefore be used to calculate the strain and strain rate experienced by the specimen by utilizing the displacement data collected by the LVDT. The effective gauge lengths for 600°C in air and in saturated steam conditions were calculated using this approach, data from the temperature profiles discussed in Section 4.1, as well as a creep activation energy of 177 kJ/mol·K for Hi-Nicalon™ S fibers, according to literature [10]. Table 6 displays the calculated effective gauge lengths for both testing conditions.

**Table 6 : Effective lengths calculated in air and saturated steam at 600°C**

|                       | Air   | Saturated Steam |
|-----------------------|-------|-----------------|
| Effective Length (mm) | 63.34 | 58.50           |

It is important to mention that there are several other methods that can be employed to observe the effective gauge length of the fiber tow specimens; however, such methods may rely on subjectivity. The method utilized for this research is based on those proposed by DiCarlo [30], Morrell [31], and Kandil and Dyson [32].

### **4.3 Static Fatigue of Hi-Nicalon™ S Fiber Tows at 600°C**

Prior to analyzing the experimental data gathered from the tensile creep tests of Hi-Nicalon™ S fiber tows at 600°C in air and silicic acid-saturated steam, a few assumptions should be mentioned. First, it is assumed that each fiber tow specimen, containing roughly 500 intact filaments, each with the same diameter (13  $\mu\text{m}$ ) and cross-sectional area, will be loaded equally. Moreover, we assume that the fibers' cross-sectional area does not change due to oxidation experienced at elevated temperatures. Although, it is recognized that production defects and specimen preparation damage, as well as oxidation of the fibers at elevated temperatures do, in fact, alter the effective cross-sectional area of the fibers, thus resulting in an increase of applied stress throughout testing.

Additionally, it is assumed that the silicic acid-saturated steam, which is delivered to the test chamber, is free of contaminants. This assumption is unlikely as the steam could be contaminated from the alumina tube that runs throughout the testing facility. Lastly, we acknowledge the difficulty associated with classifying the specimen's deformation as having been a result of creep mechanisms and not due to gradual failure. Hypothetically, there could be a small portion of fibers that are broken, significantly smaller than the majority, or defected, which would promote their failure during the creep

test prior to the specimen's complete rupture. As these hypothetically inferior fibers gradually fail, the applied load is then transferred to the remaining fibers. Consequently, the remaining fibers would experience a larger applied stress than intended which would in turn cause the increase in deformation due to stress rather than creep. Therefore, we believe the deformation behavior of the fiber tows observed in this endeavor is a result of static fatigue.

Tensile creep tests of Hi-Nicalon<sup>TM</sup> S fiber tows were performed at 600°C in laboratory air and silicic acid-saturated steam. Table 7 outlines the fiber tow specimen, testing condition, applied stress, lifetime of the fiber tow, steady-state strain rate, and percent accumulated/failure strain for each test conducted. Run-out was defined as the survival of 100 hours at applied stress.

**Table 7 : Summary of tensile static fatigue test results obtained for Hi-Nicalon™ S fiber tows at 600°C in laboratory air and in silicic acid-saturated steam**

| <b>Specimen ID</b> | <b>Test Environment</b> | <b>Applied Stress (MPa)</b> | <b>Lifetime (hrs)</b> | <b>Steady-State Strain Rate (s<sup>-1</sup>)</b> | <b>Failure Strain (%)</b> |
|--------------------|-------------------------|-----------------------------|-----------------------|--|---------------------------|
| AC8                | Air                     | 2.96                        | 100†                  | 1.41E-10   | 0.00869                   |
| AC6                | Air                     | 1023                        | 100†                  | 1.87E-09   | 0.37785                   |
| AR20               | Air                     | 1157                        | 100†                  | 7.19E-09   | 0.67891                   |
| AC29               | Air                     | 1257                        | 100†                  | 3.34E-09   | 0.32600                   |
| AC31               | Air                     | 1300                        | 100†                  | 3.97E-09   | 0.24757                   |
| SC17               | Sat. Steam              | 2.96                        | 100†                  | 3.20E-10   | 0.04163                   |
| SC26               | Sat. Steam              | 1023                        | 56.91                 | 2.66E-09   | 0.22613                   |
| SC25               | Sat. Steam              | 1157                        | 26.54                 | 1.32E-08   | 0.21287                   |
| SC22               | Sat. Steam              | 1257                        | 13.73                 | 1.29E-08   | 0.17376                   |
| SC24               | Sat. Steam              | 1300                        | 13.13                 | 1.62E-08   | 0.26122                   |

† The specimen achieved 100-h run-out, the test was terminated before specimen failure

The displacement data measured by the LVDT was used to calculate the strain for each applied stress and each environmental testing condition. Representative strain versus time curves were constructed for each applied stress value based on the calculated strain results and the time data collected by the MTS software. The representative strain versus time curves for the fiber tows tested in air and in silicic acid-saturated steam can be seen in Figure 21-24 for the applied stress of 1023 MPa, 1157 MPa, 1257 MPa, and 1300 MPa, respectively. The strain versus time curves for the case of 2.96 MPa, in both air and saturated steam, demonstrated negligible strain, as expected. This result acted as a verification tool for the test facility, tensile creep test procedure, and the material behavior of the fiber tows. It also served as a baseline for comparison of the steam test

results. The step like behavior seen especially in Figure 23 and Figure 24 for the case of 1257 MPa and 1300 MPa of applied stress, suggests the instantaneous failure of groups of fibers within the tow. This instantaneous failure of individual filaments causes redistribution of the applied load to the remaining intact fibers, resulting in the intact fibers experiencing an increase in stress and strain. Figure 25 and Figure 27 show a summary of the representative strain versus time curves for the laboratory air condition and silicic acid-saturated steam condition, respectively. All strain vs. time curves obtained in air and saturated steam displayed transient and steady-state regimes with the transition between the two regimes occurring within the first hour of each test. These regimes can be observed in Figures 26 and 28, where the time scale is truncated to highlight strain vs. time behavior during the first five hours of each test in air and saturated steam, respectively. It is clear from Table 7 and Figures 21-24 that the fiber tows tested in laboratory air accumulated larger strain than the fiber tows tested in the silicic acid-saturated steam environment.

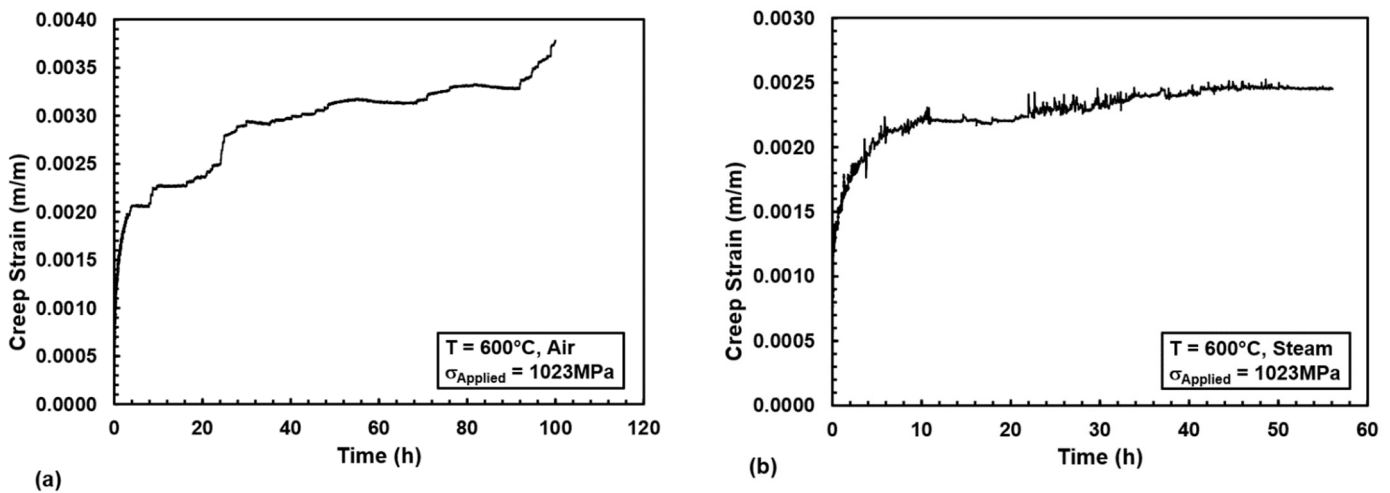


Figure 21 : Representative strain vs. time curves for Hi-Nicalon™ S fiber tows at 600°C at 1023 MPa in (a) air and (b) saturated steam

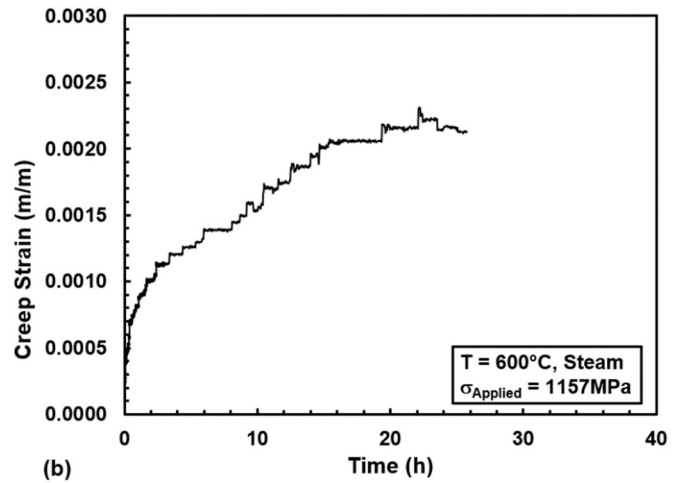
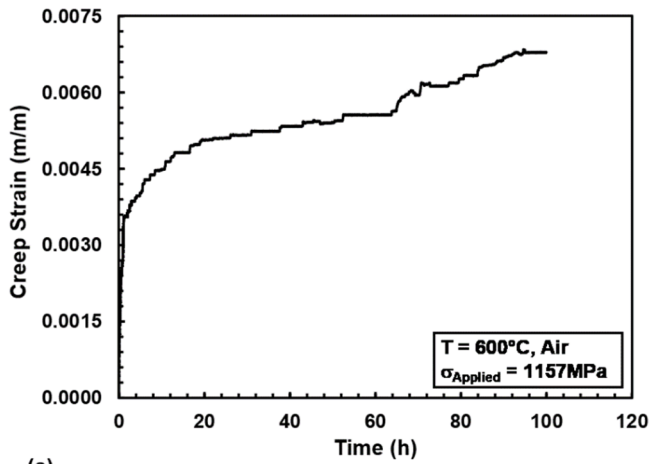


Figure 22 : Representative strain vs. time curves for Hi-Nicalon™ S fiber tows at 600°C at 1157 MPa in (a) air and (b) saturated steam

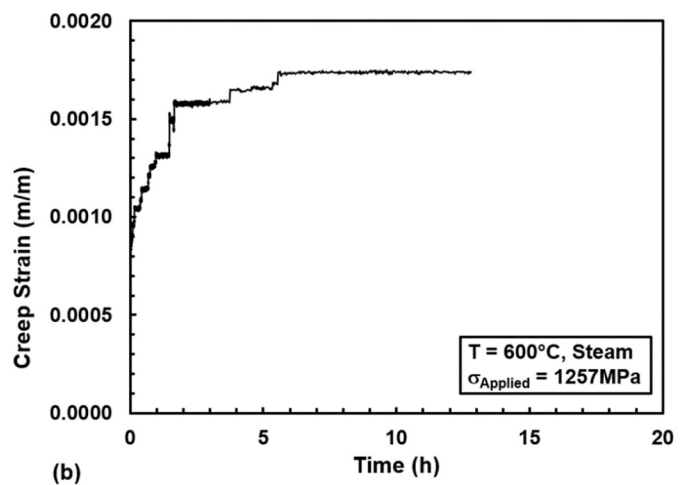
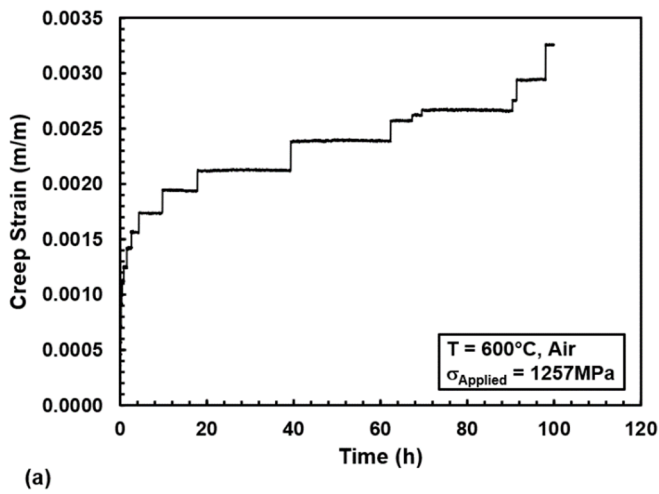


Figure 23 : Representative strain vs. time curves for Hi-Nicalon™ S fiber tows at 600°C at 1257 MPa in (a) air and (b) saturated steam

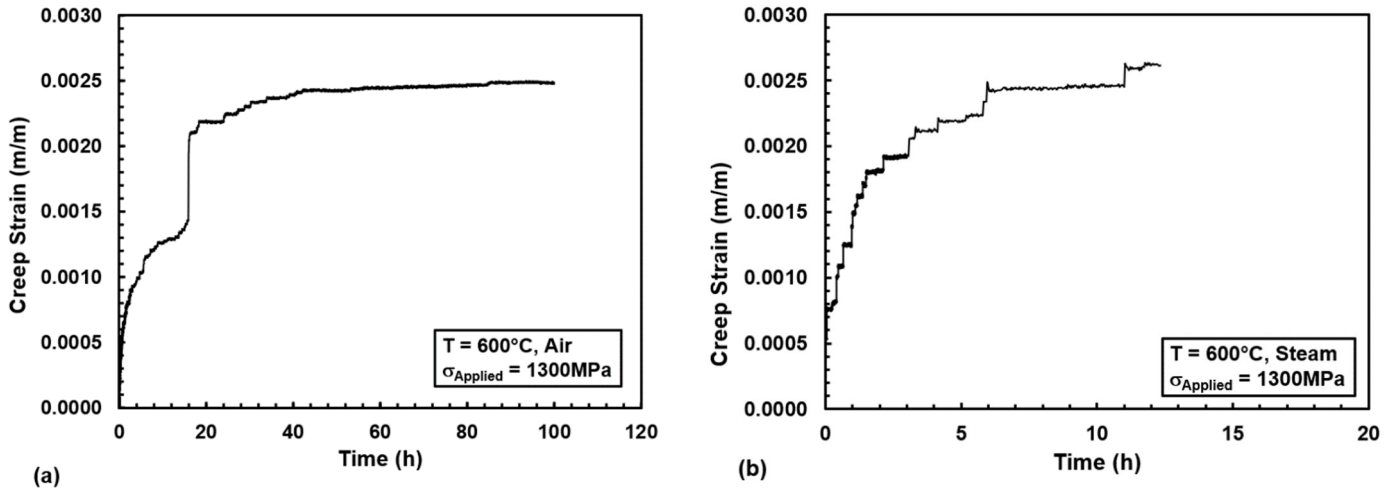


Figure 24 : Representative strain vs. time curves for Hi-Nicalon™ S fiber tows at 600°C at 1300 MPa in (a) air and (b) saturated steam

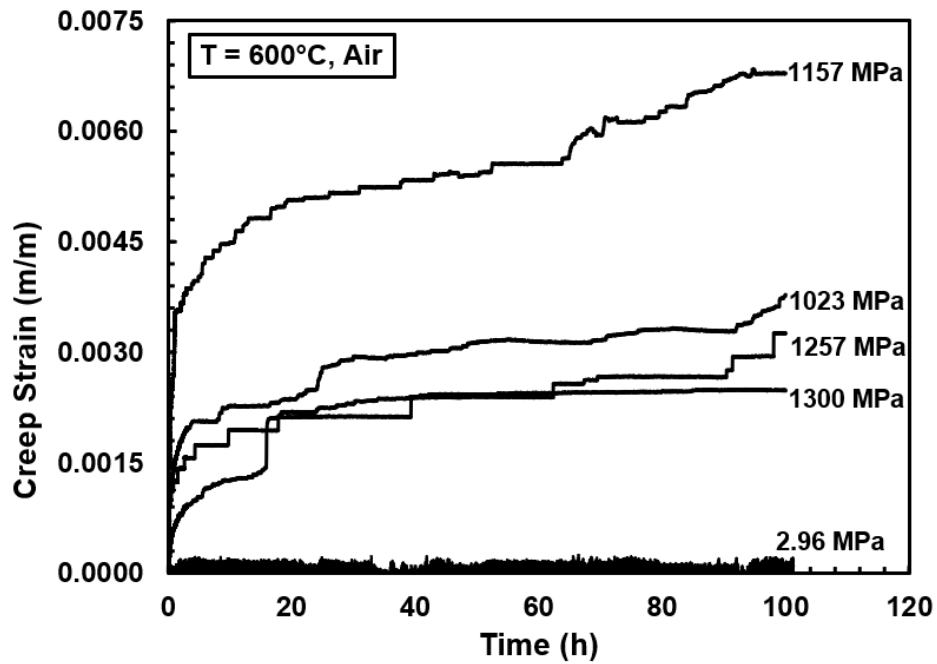


Figure 25 : Representative strain vs. time curves for Hi-Nicalon™ S fiber tows at 600°C in air

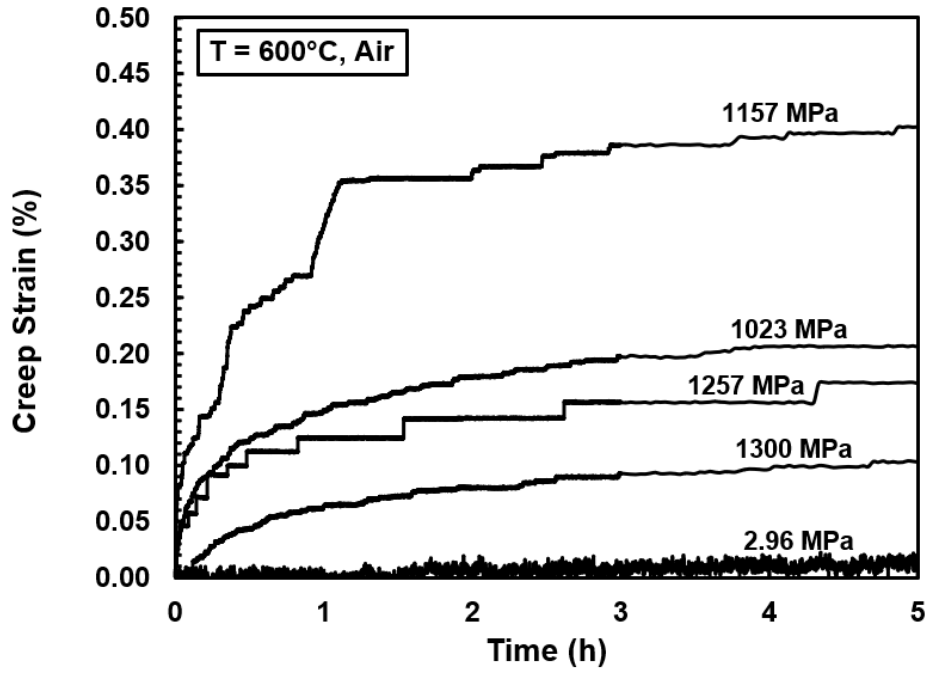


Figure 26 : Representative strain vs. time curves for Hi-Nicalon™ S fiber tows at 600°C in air. Time scale is truncated to highlight strain vs. time behavior during early portion of each test

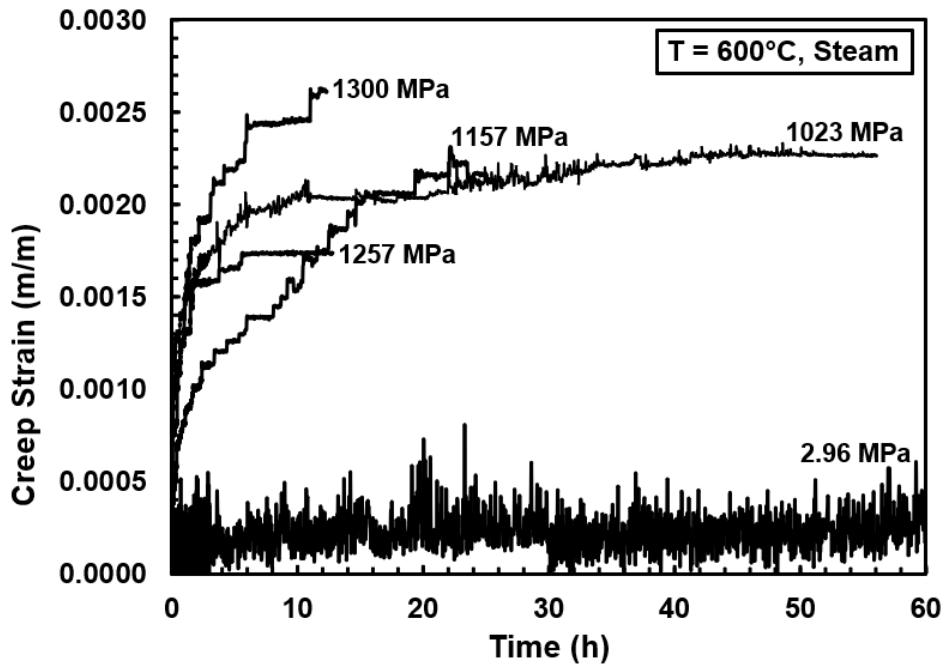


Figure 27 : Representative strain vs. time curves for Hi-Nicalon™ S fiber tows at 600°C in saturated steam

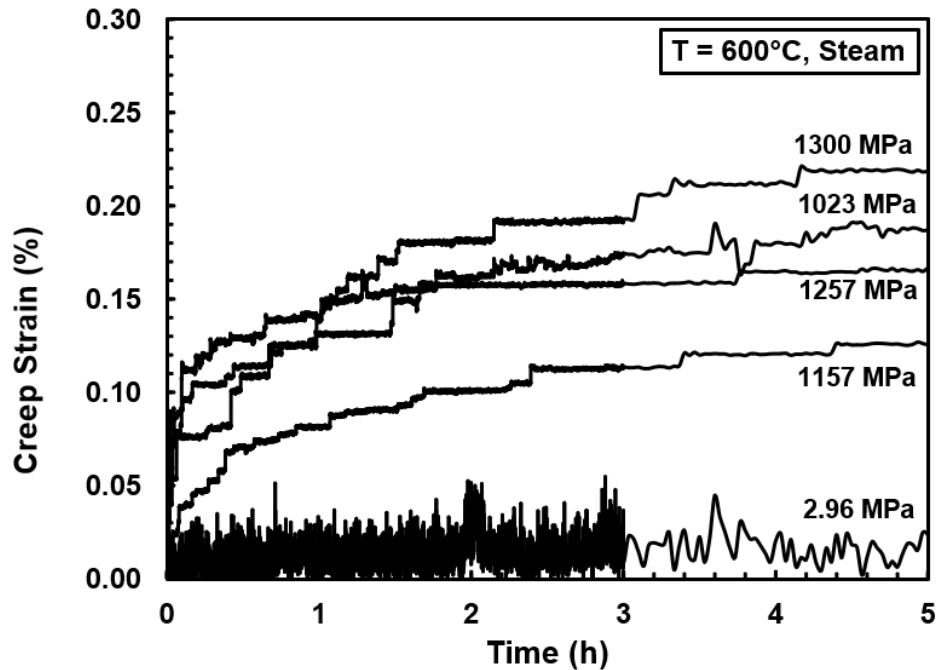


Figure 28 : Representative strain vs. time curves for Hi-Nicalon™ S fiber tows at 600°C in air. Time scale is truncated to highlight strain vs. time behavior during early portion of each test

From the representative strain versus time curves, the steady-state strain rates were extracted. The process for extracting the strain rates entailed subjectively selecting a linear portion of data and fitting a linear trendline to that selected portion. The slope of the generated trendline is the extracted strain rate for that case of applied stress. In the case of multiple seemingly linear portions of data shown, several trendlines should be fit to the data and the magnitude of each lines' slope examined to determine the overall strain rate. Table 7 lists the strain rates extracted for every specimen tested in laboratory air and silicic acid-saturated steam. As expected, the observed strain rates were extremely small. This observation is consistent with the behavior of brittle ceramic fibers. Figure 29

shows the strain rates extracted for both air and saturated steam conditions for various applied stress values.

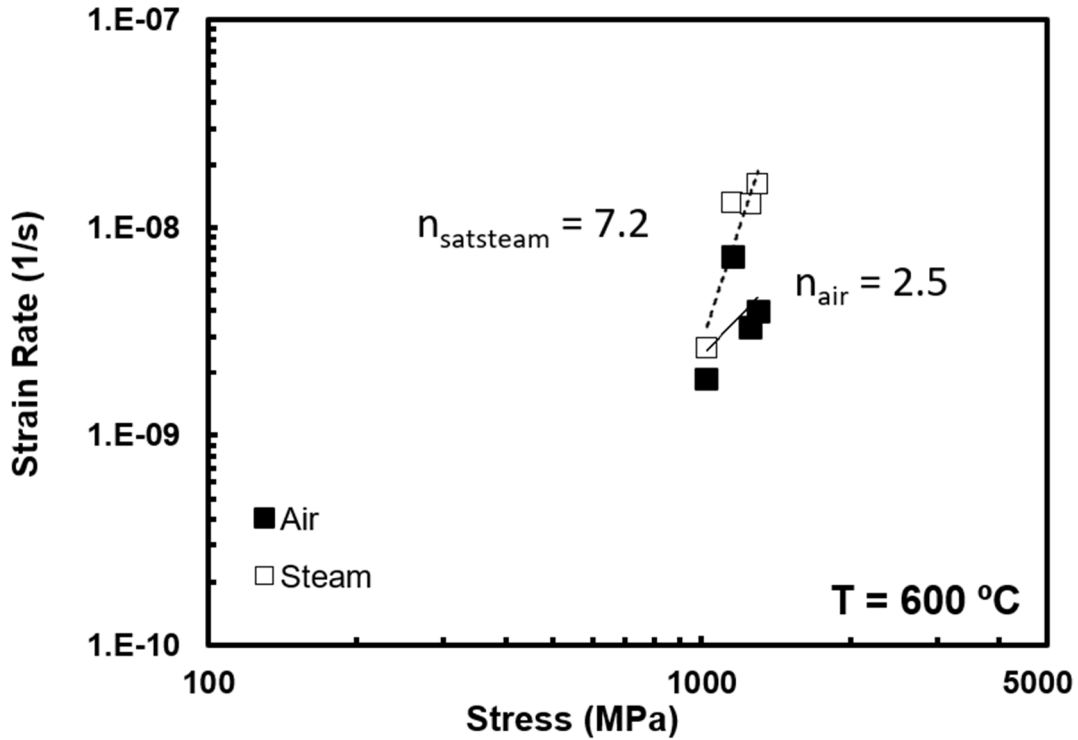


Figure 29 : Strain rates vs. applied stress for Hi-Nicalon™ S fiber tows at 600°C in both air and saturated steam

Fitting the strain rate data to a mechanical strain rate power law equation:

$$\dot{\epsilon} = A\sigma^n \quad (12)$$

where  $\dot{\epsilon}$  is the minimum creep strain rate,  $A$  is a temperature-dependent coefficient which accounts for the activation energy and other variables, and  $\sigma$  is the applied stress, allows for the variable  $n$ , also known as the stress exponent from the discussion in Section 2.3.2, to be determined. The stress exponent helps to classify the dominant creep mechanism experienced by the fibers throughout the tensile creep tests, assuming that the

deformation behavior is due to creep. As seen in Figure 29 the stress exponent for the tests conducted in air was found to be  $n \approx 2.5$ , indicating the fibers experienced grain boundary sliding and interface-reaction controlled creep as the primary mechanism, according to Table 4. The stress exponent for the tests conducted in saturated steam was found to be  $n \approx 7.2$  (Figure 29). Again, using Table 4, this value indicates the fiber tows experienced cavity growth-controlled creep as the primary creep mechanism while exposed to silicic acid-saturated steam.

The stress exponents found in this research effort for both air and saturated steam environments are similar to those found at other intermediate temperatures, such as 500, 700, and 800°C. Table 8 includes the stress exponents obtained by other AFIT researchers for tests conducted in air and silicic acid-saturated steam at 500°C [33], 700°C [23], and 800°C [17]. This finding infers that the deformation behavior of the fiber tows tested at intermediate temperatures is primarily controlled by cavity growth creep.

**Table 8 : Comparison of stress exponents obtained for the Hi-Nicalon™ S fiber tows at intermediate temperatures in air and saturated steam**

| Testing Temperature | $n_{air}$ | $n_{satsteam}$ | Creep mechanism  |
|---------------------|-----------|----------------|--|
| 500° C              | 2.4       | ‡              | Grain boundary sliding/interface-reaction                            |
| 600° C              | 2.5       | 7.2            | Grain boundary sliding/interface-reaction & Cavity growth-controlled |
| 700° C              | 5.1       | 5.3            | Cavity growth-controlled   |
| 800° C              | 5.0       | 4.1            | Cavity growth-controlled/dislocation                                 |

‡ Insufficient data to determine stress exponent

The static fatigue lifetime data gathered from tests conducted in the silicic acid-saturated steam environment in this work also concurs with previously reported results [29]. Figure 30 demonstrates that at the given stress levels, the static fatigue lifetime of the fiber tow in silicic acid-saturated steam is approximately one order of magnitude lower than that of the fiber tow in laboratory air. This observation confirms that oxidizing environments such as steam, are detrimental to the overall durability and performance of the Hi-Nicalon™ S fiber tows.

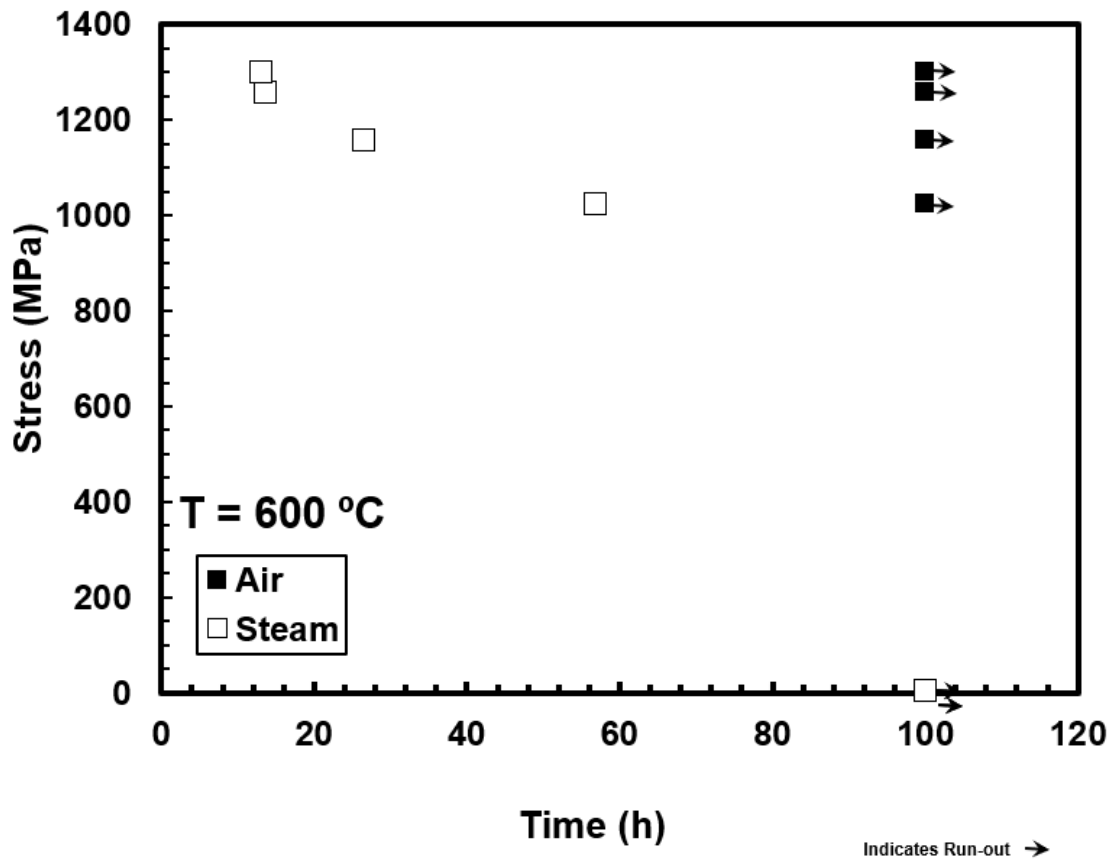


Figure 30 : Applied stress vs. time to rupture obtained for Hi-Nicalon™ S at 600°C in air and saturated steam. Arrow indicates that specimen failure did not occur when the test was terminated

As shown in Figure 30, every test conducted in laboratory air achieved run-out. This result is unlike those reported in the past theses at AFIT. For example, Piper [23], whose target temperature was 700°C, ran a test in laboratory air with an applied stress of 1257 MPa and reported the fiber tow’s lifetime to be 0.58 hours. This difference in data suggests there may exist a temperature where the static fatigue lifetimes of Hi-Nicalon™ S fiber tows are not heavily influenced by temperature in laboratory air for the stresses up to 1300 MPa. This observation was supported by the results obtained at 500°C by

Reinink [33] results, who reported 100 h lifetimes for various applied stresses at 500° C in laboratory air as well.

#### **4.4 Microstructural Analysis of Hi-Nicalon™ S Fiber Tows**

Post-test microstructural analysis of the fiber fracture surfaces, and outer surfaces is necessary to elucidate the effects of degradation due to oxidation. Optical Microscopy and Scanning Electron Microscopy (SEM) are two types of imagery analyses that are commonly used in fiber tow research. Each method of imagery aids in viewing the amount of silica scale growth seen on the fibers for the given test temperature. The observations gathered from microscopy contribute to the knowledge of Hi-Nicalon™ S fiber tow's microstructural changes occurring at elevated temperatures.

Unfortunately, due to the unforeseen challenges presented by the COVID-19 pandemic, the microscopy analyses mentioned above were not conducted on the tested fiber tow specimens. Imagery analyses will be postponed until further notice. The tested specimens were clearly labeled and placed in a secure location to await future analysis via microscopy.

## **V. Conclusions and Recommendations**

### **5.1 Conclusions**

This study investigated the static fatigue of Hi-Nicalon™ S SiC fiber tows at an intermediate temperature of 600°C in laboratory air and in silicic acid-saturated steam. The fiber tow consists of 500 fiber filaments with an average diameter of 13 μm. Static

fatigue tests were performed at applied stresses which ranged from 2.96 MPa to 1300 MPa. Run-out defined as survival of 100 h at applied stress was achieved for the entire spectrum of applied stresses in laboratory air as well as 2.96 MPa in silicic acid-saturated steam. The presence of saturated steam significantly degraded the static fatigue performance of the fiber tows at 600°C, resulting in a one order of magnitude decrease in the static fatigue lifetime of the Hi-Nicalon™ S SiC fiber tows.

If the deformation behavior were due to creep as opposed to static fatigue, then the dominant creep mechanism would be grain boundary sliding and interface-reaction controlled creep ( $n \approx 2.5$ ) for specimens tested in air, and cavity growth-controlled creep ( $n \approx 7.2$ ) for specimens tested in the saturated steam. Here  $n$  is the stress exponent found from the mechanical strain rate power law curve fit.

The results from this research were compared to those of prior work completed at AFIT; specifically, the results obtained at 500°C [33], 700°C [23], and 800°C [17]. Notably, the static fatigue lifetimes produced in saturated steam were one order magnitude lower than those produced in laboratory air. Moreover, the consistent run-out produced in laboratory air at various applied stresses at 500°C and 600°C suggests that static fatigue lifetime of the fiber tow may not be significantly affected by temperature at or below 600°C in laboratory air for the stresses up to and including 1300 MPa.

## **5.2 Recommendations for Future Research**

This research effort did not include microstructural examinations and analyses such as scanning electron microscopy (SEM), optical microscopy, and transmission electron microscopy (TEM) of the tested fiber tow specimens due to unforeseen

challenges presented by the COVID-19 pandemic. Further microstructural investigation of the fiber fracture surfaces would contribute to the understanding of the oxidation and degradation of Hi-Nicalon<sup>TM</sup> S SiC fiber tows in the presence of silicic acid-saturated steam environments. Noting the type of oxidation, passive or active, that occurred on the surface of the fibers by examining the existence or absence of silica scale growth would further contribute to the understanding of the Hi-Nicalon<sup>TM</sup> S fiber tows static fatigue lifetime and mechanical behavior at intermediate temperatures.

It should be noted that the equipment used to accomplish this work was not inherently accurate or reliable. The output of the furnaces, preheaters, and the steam generator did not represent the commanded input; thus, it was challenging to select correct and repeatable temperature settings for the tests. Upgrading or changing out the hardware would not only allow for the ability to test at higher temperatures, but it would also alleviate the inconsistent and large temperature variations collected by the thermocouples located at the bleed-off assembly and within the furnaces. Future efforts would greatly benefit from more reliable equipment and a testing procedure that did not incorporate as many moving parts.

## Bibliography

- [1] Not Measurement Sensitive Mil-Hdbk, “DEPARTMENT OF DEFENSE HANDBOOK COMPOSITE MATERIALS HANDBOOK VOLUME 5. CERAMIC MATRIX COMPOSITES AMSC N/A AREA CMPS DISTRIBUTION STATEMENT A. Approved for public release; distribution unlimited,” 2002.
- [2] “Johnson T\_history\_of\_composites.”
- [3] S. Schmidt, S. Beyer, H. Knabe, H. Immich, R. Meistring, and A. Gessler, “Advanced ceramic matrix composite materials for current and future propulsion technology applications,” in *Acta Astronautica*, Aug. 2004, vol. 55, no. 3–9, pp. 409–420, doi: 10.1016/j.actaastro.2004.05.052.
- [4] C. Armani, “Creep performance of oxide ceramic fiber materials at elevated temperature in air and in steam,” 2011, [Online]. Available: <http://oai.dtic.mil/oai/oai?verb=getRecord&metadataPrefix=html&identifier=ADA538514>.
- [5] M. Braginsky and C. P. Przybyla, “Simulation of crack propagation/deflection in ceramic matrix continuous fiber reinforced composites with weak interphase via the extended finite element method,” *Compos. Struct.*, vol. 136, pp. 538–545, 2016, doi: 10.1016/j.compstruct.2015.10.038.
- [6] K. K. Chawla, *Ceramic Matrix Composites*. 2003.
- [7] N. E. Dowling, *Mechanical Behavior of Materials: Engineering Methods for Deformation, Fracture, and Fatigue*, 4th ed. Pearson, 2012.

- [8] F. W. Zok, "Developments in oxide fiber composites," *J. Am. Ceram. Soc.*, vol. 89, no. 11, pp. 3309–3324, 2006, doi: 10.1111/j.1551-2916.2006.01342.x.
- [9] J. J. Sha, J. S. Park, T. Hinoki, and A. Kohyama, "Heat treatment effects on creep behavior of polycrystalline SiC fibers," *Mater. Charact.*, vol. 57, no. 1, pp. 6–11, 2006, doi: 10.1016/j.matchar.2005.11.019.
- [10] W. Gauthier and J. Lamon, "Delayed failure of hi-nicalon and hi-nicalon s multifilament tows and single filaments at intermediate temperatures (500°-800°C)," *J. Am. Ceram. Soc.*, vol. 92, no. 3, pp. 702–709, Mar. 2009, doi: 10.1111/j.1551-2916.2009.02924.x.
- [11] A. R. Bunsell and A. Piant, "A review of the development of three generations of small diameter silicon carbide fibres," *J. Mater. Sci.*, vol. 41, no. 3, pp. 823–839, 2006, doi: 10.1007/s10853-006-6566-z.
- [12] L. Gumucio, "CREEP OF HI-NICALON™ S CERAMIC FIBER TOWS AT 1100°C IN AIR AND IN SILICIC ACID-SATURATED STEAM," Air Force Institute of Technology, 2018.
- [13] T. Ishikawa, "Advanced in Inorganic Fibers," in *Advances in Polymer Science*, 2005, pp. 109–144.
- [14] W. Gauthier, F. Pailler, J. Lamon, and R. Pailler, "Oxidation of silicon carbide fibers during static fatigue in air at intermediate temperatures," *J. Am. Ceram. Soc.*, vol. 92, no. 9, pp. 2067–2073, Sep. 2009, doi: 10.1111/j.1551-2916.2009.03180.x.
- [15] M. C. Halbig and A. J. Eckel, "Oxidation of Continuous Carbon Fibers Within a

- Silicon Carbide Matrix Under Stressed and Unstressed Conditions,” 2000.  
[Online]. Available: <http://www.sti.nasa.gov>.
- [16] R. S. Hay and R. Corns, “Passive oxidation kinetics for glass and cristobalite formation on Hi-Nicalon<sup>TM</sup>-S SiC fibers in steam,” *J. Am. Ceram. Soc.*, vol. 101, no. 11, pp. 5241–5256, 2018, doi: 10.1111/jace.15763.
- [17] S. J. Robertson, “Air Force Institute of Technology Architecture,” *Inf. Secur.*, no. September, 2006.
- [18] M. Wachtman, J., Cannon, W., Matthewson, *Mechanical Properties of Ceramics*, 2nd ed. New York: John Wiley & Sons Inc., 2009.
- [19] J. P. Poirier, *Creep of Crystals*. New York, NY: Cambridge University Press, 1985.
- [20] S. Benjamin, “CREEP OF HI-NICALON S CERAMIC FIBER TOWS AT ELEVATED TEMPERATURE IN AIR AND IN STEAM,” 2012.
- [21] T. R. Shillig, “Creep of Hi-Nicalon S Fiber Tows At Elevated Temperature in Air and in Steam,” 2013.
- [22] K. Sprinkle, “CREEP OF SYLRAMIC-iBN FIBER TOWS AT ELEVATED TEMPERATURE IN AIR AND IN SILICIC ACID-SATURATED STEAM,” Air Force Institute of Technology, 2015.
- [23] M. Piper, “CREEP OF HI-NICALON<sup>TM</sup> S CERAMIC FIBER TOWS AT 700°C IN AIR AND IN SILICIC ACID-SATURATED STEAM,” Air Force Institute of Technology, 2016.
- [24] R. Mitchell, “CREEP OF HI-NICALON<sup>TM</sup> S CERAMIC FIBER TOWS AT

- 900°C IN AIR AND IN SILICIC ACID-SATURATED STEAM,” The Air Force Institute of Technology, 2017.
- [25] B. Kroeger, “CREEP OF HI-NICALON™ S CERAMIC FIBER TOWS AT 1000°C IN AIR AND IN SILICIC ACID-SATURATED STEAM,” Air Force Institute of Technology, 2018.
- [26] C. Profile, P. Information, and O. P. Information, “Silicon Carbide Continuous Fibers,” 2020. .
- [27] C. I. COI, “HI-NICALON Type S CERAMIC FIBER,” *Ratio*, 1999.  
[http://www.coiceramics.com/pdfs/hi-nicalon-types\\_1-17-06.pdf](http://www.coiceramics.com/pdfs/hi-nicalon-types_1-17-06.pdf) (accessed Sep. 29, 2020).
- [28] N. G. S. Advanced and F. Co, “Product | NGS Advanced Fibers Co., Ltd.,” 2020. .
- [29] S. J. Robertson *et al.*, “Static fatigue of Hi-Nicalon™-S fiber at elevated temperature in air, steam, and silicic acid-saturated steam,” *J. Am. Ceram. Soc.*, vol. 103, no. 2, pp. 1358–1371, 2020, doi: 10.1111/jace.16799.
- [30] J. A. DiCarlo, “Property goals and test methods for high temperature ceramic fibre reinforcement,” *Ceram. Int.*, vol. 23, no. 4, pp. 283–289, 1997, doi: 10.1016/S0272-8842(96)00007-7.
- [31] R. M. Morrell, “A tensile creep-testing apparatus for ceramic materials using simple knife-edge universal joints,” *J. Phys. E.*, vol. 5, no. 5, pp. 465–467, 1972, doi: 10.1088/0022-3735/5/5/028.
- [32] F. A. Kandil and B. F. Dyson, “Tensile creep of ceramics: the development of a testing facility,” *Int. J. High Technol. Ceram.*, vol. 4, no. 2–4, pp. 243–262, 1988,

doi: 10.1016/0267-3762(88)90048-3.

- [33] R. Reinink, "STATIC FATIGUE OF HI-NICALON™ S CERAMIC FIBER TOWS AT 500°C IN AIR AND SILICIC ACID-SATURATED STEAM," The Air Force Institute of Technology, 2021.

| <b>REPORT DOCUMENTATION PAGE</b>   |                             |  | <i>Form Approved</i><br>OMB No. 074-0188   |  |
|--|-----------------------------|--|--|--|
| The public reporting burden for this collection of information is estimated to average 1 hour per response, including the time for reviewing instructions, searching existing data sources, gathering and maintaining the data needed, and completing and reviewing the collection of information. Send comments regarding this burden estimate or any other aspect of the collection of information, including suggestions for reducing this burden to Department of Defense, Washington Headquarters Services, Directorate for Information Operations and Reports (0704-0188), 1215 Jefferson Davis Highway, Suite 1204, Arlington, VA 22202-4302. Respondents should be aware that notwithstanding any other provision of law, no person shall be subject to a penalty for failing to comply with a collection of information if it does not display a currently valid OMB control number.  |                             |  |  |  |
| <b>PLEASE DO NOT RETURN YOUR FORM TO THE ABOVE ADDRESS.</b>  |                             |  |  |  |
| <b>1. REPORT DATE (DD-MM-YYYY)</b><br>25-03-2021   |                             | <b>2. REPORT TYPE</b><br>Graduate Research Paper |  | <b>3. DATES COVERED (From – To)</b><br>September 2019 – March 2021 |
| <b>TITLE AND SUBTITLE</b><br><br>STATIC FATIGUE OF HI-NICALON™ S CERAMIC FIBER TOWS AT 600°C IN AIR AND SILICIC ACID-SATURATED STEAM   |                             |  | <b>5a. CONTRACT NUMBER</b>   |  |
|  |                             |  | <b>5b. GRANT NUMBER</b>  |  |
|  |                             |  | <b>5c. PROGRAM ELEMENT NUMBER</b>  |  |
| <b>6. AUTHOR(S)</b><br><br>Nelson, Caleigh M., Second Lieutenant, USAF   |                             |  | <b>5d. PROJECT NUMBER</b>  |  |
|  |                             |  | <b>5e. TASK NUMBER</b>   |  |
|  |                             |  | <b>5f. WORK UNIT NUMBER</b>  |  |
| <b>7. PERFORMING ORGANIZATION NAMES(S) AND ADDRESS(S)</b><br>Air Force Institute of Technology<br>Graduate School of Engineering and Management (AFIT/ENY)<br>2950 Hobson Way, Building 640<br>WPAFB OH 45433-8865   |                             |  | <b>8. PERFORMING ORGANIZATION REPORT NUMBER</b><br><br>AFIT-ENY-MS-21-M-309                                    |  |
| <b>9. SPONSORING/MONITORING AGENCY NAME(S) AND ADDRESS(ES)</b><br>Intentionally left blank   |                             |  | <b>10. SPONSOR/MONITOR'S ACRONYM(S)</b>  |  |
|  |                             |  | <b>11. SPONSOR/MONITOR'S REPORT</b>  |  |
| <b>12. DISTRIBUTION/AVAILABILITY STATEMENT</b><br>DISTRUBTION STATEMENT A. APPROVED FOR PUBLIC RELEASE; DISTRIBUTION UNLIMITED.  |                             |  |  |  |
| <b>13. SUPPLEMENTARY NOTES</b><br>This material is declared a work of the U.S. Government and is not subject to copyright protection in the United States.   |                             |  |  |  |
| <b>14. ABSTRACT</b><br><br>Ceramic matrix composites (CMCs) have the potential to be utilized in applications such as hypersonic vehicles, aircraft leading edges, hot sections of engines, and rocket nozzles. Of particular interest are advanced SiC/SiC composites that can withstand the elevated temperatures and harsh oxidizing environments while maintaining their properties and structural integrity under an applied load. Steam, a major component of combustion environment, is one such aggressive oxidizing environment. As steam passes through the SiC/SiC composite, entering the composite interior through the cracks in the SiC matrix, it becomes saturated with silicic acid, Si(OH) <sub>4</sub> . Before incorporating SiC/SiC composites in the next generation aerospace engines, the long-term impacts of exposure to the aggressive saturated steam environment on the composite durability must be thoroughly examined and understood. An in-depth understanding of the composite performance demands an in-depth study and understanding of the performance of the reinforcing SiC fibers. This study investigates the static fatigue of Hi-Nicalon™ S SiC fiber tows at an intermediate temperature of 600°C in laboratory air and in silicic acid-saturated steam. The fiber tow consists of 500 fiber filaments with an average diameter of 13 μm. Static fatigue tests were performed at applied stresses ranging from 2.96 MPa to 1300 MPa. Run-out was defined as survival of 100 h at applied stress. The presence of saturated steam significantly degraded the static fatigue performance of the fiber tows at 600°C. The static fatigue lifetimes of the Hi-Nicalon™ S SiC fiber tows were decreased by one order of magnitude due to silicic acid-saturated steam. |                             |  |  |  |
| <b>15. SUBJECT TERMS</b><br>Hi-Nicalon™ S, SiC fiber tows, ceramic fibers, creep, tension, steam environment, oxidation, static fatigue  |                             |  |  |  |
| <b>16. SECURITY CLASSIFICATION OF:</b>   |                             |  | <b>17. LIMITATION OF ABSTRACT</b><br><br>UU  | <b>18. NUMBER OF PAGES</b><br><br>61                               |
| <b>a. REPORT</b><br><br>U  | <b>b. ABSTRACT</b><br><br>U | <b>c. THIS PAGE</b><br><br>U                     |  |  |
|  |                             |  | <b>19b. TELEPHONE NUMBER (Include area code)</b><br>(937) 255-3636 ext. 4641<br>(marina.ruggleswrenn@afit.edu) |  |